# Multi-objective optimization of building-integrated microalgae photobioreactors for energy and daylighting performance

Talaei, Maryam; Mahdavinejad, Mohammadjavad; Azari, Rahman; Prieto Hoces, A.I.; Sangin, Hamed

**DOI**
10.1016/j.jobe.2021.102832

**Publication date**
2021

**Document Version**
Final published version

**Published in**
Journal of Building Engineering

Journal of Building Engineering 42 (2021) 102832

Contents lists available at ScienceDirect

Journal of Building Engineering

journal homepage: www.elsevier.com/locate/jobe

# Multi-objective optimization of building-integrated microalgae photobioreactors for energy and daylighting performance

Maryam Talaei [a], Mohammadjavad Mahdavinejad [a,*], Rahman Azari [b], Alejandro Prieto [c], Hamed Sangin [d]

[a] Department of Architecture, Faculty of Art and Architecture, Tarbiat Modares University, Jalal-Ale Ahmad Street, 14115-111, Tehran, Iran
[b] College of Arts and Architecture, Pennsylvania State University, State College, PA, 16801, United States
[c] Delft University of Technology, Faculty of Architecture and the Built Environment, Department of Architectural Engineering + Technology, Architectural Façades & Products Research Group, Julianalaan 134, 2628BL, Delft, the Netherlands
[d] College of Architecture and Urban Design, Tehran University of Art, Sakhai St., Hafez Ave., 1136813518, Tehran, Iran

ARTICLE INFO

*Keywords:*
Multi-objective optimization
Daylighting performance
Energy efficiency
Microalgae bioreactor
Building façade
Green envelop

ABSTRACT

As a state-of-the-art green façade technology, building-integrated microalgae bioreactor has the potential to reduce buildings' carbon footprint and energy consumption. The present study aims to address the knowledge gap in the energy and daylighting performance of algae photobioreactor façade. The paper first studies the effects of algae windows on building energy saving through simulation analysis of an office building in Mashhad, Iran, with a cold semi-arid climate. It also presents a multi-objective optimization framework for the optimization of the energy and daylighting performance of algae windows integrated with an office building facade. Two optimization metrics include maximum Useful Daylight Illuminance (UDI) (%), and minimum Energy Use Intensity (EUI) (kWh/m$^2$/yr), representing optimal daylighting and energy performance metrics, respectively. The results demonstrate that a microalgae window significantly reduces building energy consumption comparing with single-glazed, double-glazed, and water windows. The extent of energy savings varies with window size, algae density, and façade orientation. The proposed optimization framework helps increase the average values of energy performance metrics by 21.37%, 33.25%, 36.22%, 39.67%, and daylighting metrics by 4.60%, 14.43%, 13.34%,14.33%, in the north, south, east, and west, respectively and sequentially. Sensitivity analysis demonstrates that window size has the highest effect on two studied performance metrics for all orientations, while algae density has minimal effect on energy consumption and no considerable effect on daylighting performance. Building energy performance simulation is validated by ASHRAE140-2017.

## 1. Introduction

The building sector is responsible for more than one-third of the global total energy consumption and about 40% of $CO_2$ emissions [1], and various technologies, such as solar facades [2–4], climate-adaptive building shells [5], and algae façades [6,7], have been applied to reduce the energy demand and carbon footprint of buildings. The algae façade as a green façade system, as a recently-emerged technology, has received significant attention in the field of high-performance buildings [8], and integrating microalgae culture systems into buildings is believed to offer advantages such as a reduced ecological footprint [8–10], bio-fuel production [11–16], decreased energy consumption in both building and bioreactor [6,17,18], adaptable shading [19,20], acoustical insulation, and economic and environmental viability [8,9]. The symbiosis between the microalgae culture system and the building can also be beneficial for medical purposes [21], human food [22] and animal feed production [23], wastewater treatment [24,25], and production of bio-products [26] as well as energy [27]. Yet, there have been few attempts to integrate algae bioreactors into building envelopes as a kind of green façades [28] for thermal regulation [29], despite there are numerous researches on green building envelopes in terms of thermal and energy performance [30–33]. Besides, this technology is still in its

* Corresponding author. Department of Architecture, Faculty of Art and Architecture, Tarbiat Modares University, # 305, Second Floor, Post Box: 14115, Tehran, 1411713116, Iran.
*E-mail addresses:* m-talaei@modares.ac.ir (M. Talaei), mahdavinejad@modares.ac.ir (M. Mahdavinejad), razari@psu.edu (R. Azari), A.I.PrietoHoces@tudelft.nl (A. Prieto), Hamed.sangin@gmail.com (H. Sangin).

https://doi.org/10.1016/j.jobe.2021.102832
Received 12 February 2021; Received in revised form 28 May 2021; Accepted 1 June 2021
Available online 5 June 2021

infancy stages [8] in both research and development, and numerous challenges remain to be addressed before the wider application of this technology.

Previous research has examined the microalgae bioreactors from energy [34] and environmental aspects [35] and addressed some application challenges. Using experimental techniques, Umdu et al. [36] evaluated the interrelations between the U-value, and the thicknesses of the reservoir, air layer, and reservoir wall, in a flat-panel bioreactor. They concluded that air layer thickness has the highest contribution to the U-value. Pruvost et al. [6] studied a flat-panel bioreactor to define how the integration of a photobioreactor (PBR) into the building can affect its operation. Their study showed that the symbiosis between PBR and building façade can considerably reduce the energy demand for microalgal culture, in comparison to solar standalone bioreactors [6]. Kerner et al. [37] developed a system to provide optimum conditions for producing microalgae and heat. They showed that 80% of the heat produced by the PBR façade can be utilized for the building's heat supply system. Negev et al. [29] studied the effects of a microalgae bioreactor on the energy consumption of buildings in the Mediterranean climate. Through an experiment, they measured U-value, Solar Heat Gain Coefficient (SHGC), and visible transmittance (VT) of an algae window and studied how the algae concentration, window size, and combination of algae concentration and window size could reduce energy consumption. The results showed that incorporating algae windows into building façade, mostly in west and south orientations, leads to energy savings, as compared with single- and double-glazing windows. L. Pagliolico et al. [38] studied microalgae photobioreactor as a shading system (PBS) through an experiment in a real building, a kindergarten classroom, and identified 0.75 as the reference $T_v$ for this system. They also calculated the daylight amount in the room and energy demand for lighting $ED_l$ by Diva simulations comparing the results with a traditional Venetian blind in different locations. According to the simulation phase, daylight amount and the $ED_l$ for PBS and the VB showed slightly better results for PBS in Turin and Athens and slightly better results for the VB in Ostersund and Abu Dhabi. Lo Verso et al. [39] presented a case study applying PBR as a shading system for an external workspace located on an open terrace of the State Library of Queensland (SLQ) in Brisbane. They realized two main objectives; describing the application of the specifically designed PBR system and assessing the daylight performance of the outdoor space where the PBR system is installed. To encounter fluctuating weather conditions and direct sunlight and provide visual comfort for the work environment, various biomass densities were adjusted to provide a wide range of light transmittance (in the Tv = 10%–80% range). Daylighting performance of the workplace was analyzed by calculating the distribution of illuminance values inside the workspace using DIVA-for-Rhino, for different range of $T_v$. They also calculated daylighting metrics such as the Daylight Autonomy and Useful Daylight Illuminance and compared the results with two other climates (Turin, Italy, and Dubai, United Arab Emirates), to verify the system's performance under various environmental conditions. The daylighting results showed that to remain in the 'optimal' comfort range in clear sky, the maximum Tv of PBRs results should be in the range 5%–20% and to remain in the 'acceptable' comfort range Tv should be in the range 20%–30%. For overcast sky conditions, the maximum Tv of PBRs resulted in the range 40%–80% to remain in the 'optimal' comfort range. In overcast sky the maximum Tv of PBR resulted in the range 40%–80% to remain in the 'optimal' comfort range and for 'acceptable' comfort range the maximum value of 80% was suggested.

Despite previous research, a framework for the optimization of parameters affecting the environmental performance of PBR facades is missing in the field. Since optimization is a mathematical process for finding the minimum or maximum values of given functions and evaluating the design and decision options based on the 'best combination' of variables, it can complement the building performance simulation techniques and serve as a useful tool in the early stages of the architectural design of buildings to investigate design possibilities that yield the optimum objectives, as defined by project stakeholders [40]. Previous building energy and daylighting performance optimization studies have focused on variables such as window-to-wall ratio, glazing materials, shading types, materials, dimensions, and building orientation [41–48]. In Table 1, summarized the literature reviewed in the present study on multi-objective optimization for improving building performance.

No previous study has tried to optimize building-integrated PBR parameters for high daylight availability and low energy use. Moreover, the thermal performance and energy-saving potentials of PBR systems have not yet been evaluated in various climates. This research, for the first time, aims to fill these knowledge gaps, accordingly, it has two key objectives. The first objective is to analyze the thermal performance of algae culture system used in an office building facade for different building orientations, in the BSk (cold, semi-arid) climate, according to the Köppen climate classification, and comparing the results with those reported by previous studies for the Csa (hot-summer Mediterranean) climate to evaluate the performance of this innovative system under various environmental conditions. The second objective of this research is to define a framework for multi-objective optimization of algae façades for energy and daylighting performance. The proposed optimization framework incorporates parametric design, integrated energy-daylighting simulation, and Pareto fronts definition. Using the case study for pilot-testing, the optimized design solutions for all four orientations (North, South, East, West) are proposed and their characteristics are compared. Finally, sensitivity analysis is applied to evaluate the sensitivity of design variables to performance metrics. Applying ASHRAE Standard 140–2017 [62], this study evaluated and validated the accuracy of simulation software results by comparison method.

## 2. Material and methods

The research pursues three main steps to develop the proposed framework, as illustrated in Fig. 1. Step 1 is the model definition, in which the design variables of interest for simulation and optimization were identified and the initial parametric geometry model was generated. Step 2 is energy performance simulation, in which the energy use intensity (EUI) of the models for a different combination of design variables was evaluated for North, South, East, and West orientations. This step aimed to examine the effects of algae concentration and window-to-wall ratio on energy use intensity, based on four main building orientations, and compare potential energy savings achieved by algae windows with standard models using Single-Glazed (SG-Win), Double-Glazed (DG-Win), and Water-window (Water-Win = Algae 0%) systems. Step 2 also involved analyzing and comparing the energy performance in two climates: a cold semi-arid climate (BSk) and a hot-summer Mediterranean climate (Csa). Therefore, the energy use intensity results for algae-window, SG-Win, DG-Win, and Water-Win systems studied in this research for cold semi-arid climate were compared with those for the hot summer Mediterranean climate, as reported by Negev et al. [29]. Finally, step 3, multi-objective optimization including two methods, employed the multi-objective optimization technique to find the design combination, based on different algae window scenarios for four main building orientations in the BSk climate, for maximum useful daylight illuminance (UDI) and minimum energy use intensity of an office environment. The optimized design options were accordingly suggested, and a sensitivity analysis was applied to study the sensitivity of performance metrics. The independent variables for optimizations included window-to-wall ratio and algae concentration. In this research, the first method for the optimization process includes simulating design solutions and investigating Pareto optimum solutions by using the Utopian point method applied for multi-objective optimization [63,64], while the second method was conducted based on an evolutionary algorithm to evaluate the first process and enhance the methodology.

**Table 1**
Literature on multi-objective optimization of the building performance design.

| References | Location | Building | Performance metrics | Design parameters | Simulation & Optimization method Tools |
|---|---|---|---|---|---|
| [49] | Tehran, Iran | Office | Quality of view energy performance, daylighting | Window size and location | Ladybug + EnergyPlus + Octopus |
| [50] | Palermo, Torino, Italy; Frankfurt, Germany; Oslo, Norway | Office | Energy consumption (heating, cooling, lighting) | Number, position, shape, and type of windows, thickness of the masonry wall | Non-dominated Sorting Genetic Algorithm (NSGA-II) + EnergyPlus |
| [51] | Seoul, Korea | Office | Energy saving | Orientation, Slat angle in blinds, Window-to-wall ratio | EnergyPlus + DOE-2+ BLAST Multi-factor combination exploration |
| [40] | Miami, Atlanta, Chicago, USA | Office | Daylight, energy performance | Building geometry, window and skylight size and placement | EnergyPlus + Radiance + Octopus |
| [52] | The Netherlands | Office | Daylight, energy performance | Window-to-wall ratio, thermophysical and optical material properties | Genetic Algorithm |
| [53] | Korea | Office | Heating, cooling loads | Floor area, building orientation, ceiling height, aspect ratio, plenum height, window-to-wall ratio, wall insulation, window insulation, solar heat gain coefficient, air leakage | NSGA-II + TRNSYS |
| [54] | Helsinki, Finland | Residential | Thermal performance, Life-cycle-cost | Envelope insulation thickness of the external wall, roof, floor, window type, building tightness, a heat-recovery unit | MATLAB, TRNSYS, NSGA-II |
| [55] | Ankara, turkey | Library | Daylight, energy performance | Building form, spatial layout, orientation, envelope articulation | Multi-objective Architectural Design Explorer (MADE)+ Open Studio + EnergyPlus |
| [41] | China | School | Energy use, summer discomfort, Daylight illuminance | Building orientation, building shape, Window-to-wall ratio, glazing material, and shading types | EnergyPlus + Radiance + Octopus |
| [56] | Xi'an, China | Office | Energy efficiency, visual, thermal comfort | Window-to-wall ratio, outer and inner glass metrical, and the filling gas | NSGA-II + TRNSYS + Artificial Neural Network (ANN) |
| [57] | Athens, Greece | Office | Energy consumption, adaptive thermal comfort | Window-to-wall ratio, wall U-value, glazing construction U-value, glazing g-value, air-tightness of the facade, cooling set-point of the mechanical cooling system and PV facade surface area | DesignBuilder + EnergyPlus + mode-Frontier + Daysim |
| [58] | Canada | Residential | Thermal comfort and energy consumption | HVAC system settings, thermostat programming, and passive solar design | ANN prediction model + GA + TRNSYS |
| [59] | Brisbane, Darwin, Hobart and Melbourne, Australia | Commercial | Energy Saving | Building envelops and orientation | Ant colony optimization (ACOR) + EnergyPlus |
| [60] | Cairo, Egypt | Heritage palace | Thermal, visual performance | Skylight configuration | Octopus + Diva-grasshopper + ArchSim |
| [61] | Marrakech, Morocco | Residential | Thermal comfort, energy performance | Building envelope characteristics | Artificial Neural Networks (ANNs)+ Feedforward Neural Networks (MFNN), NSGA-II + Multi-Objective Particle Swarm Optimization (MOPSO)+ Multi-Objective Genetic Algorithm (MOGA)+ TRNSYS |

### 2.1. Simulation

In this research, the energy simulation outputs include annual energy loads related to lighting, heating, cooling, and electrical equipment. Also, the energy use intensity (EUI) in kWh/$m^2$/yr, which is defined as the summation of these loads divided by the building gross floor area, is used as the normalized building energy performance metric [40,65,66]. The other performance metric used in this research is UDI which is unitless and aims to determine the useful daylight levels for building occupants as a condition that is not too dark (<100 lx) or too bright (>2000 lx) [67]. UDI is the ratio of the number of hours throughout a year when daylight illuminances are within the useful range of 100–2000 lx to the total number of occupied hours in a year [68]. In this research, the two performance metrics are used simultaneously to find design options that provide a high level of daylight availability while leading to low energy consumption.

Daylighting and energy simulation were integrated into this step of research. Integrating lighting and energy simulation means that the savings in lighting, heating, cooling, electrical equipment energy use as caused by daylighting are fully considered in the energy simulation process [40]. This would require the application of a light control system in building models in which lighting systems turn off when the inner space receives sufficient daylighting for specific activities or otherwise turns on. Daylight simulation provides hourly illuminances for specific lighting sensor positions, based on which electrical lighting is adjusted to be dimmed or turned off depending on the illuminance adequacy for specific spaces and tasks. The process leads to generating a lighting schedule for the entire year. The lighting schedule is imported to the energy model to integrate lighting, cooling, heating, and equipment energy consumption based on daylighting. The size of the spatial grid cells for placement of daylighting sensors to calculate UDI was assumed to be about 0.5 × 0.5 m, placed at 0.8 m above the floor in the parametric model.

The simulation and optimization process initiates in the 3D Software Rhino and Grasshopper as a parametric modeling tool [69] to generate geometry models with pre-determined WWR, whose values can change by sliders. Moreover, the microalgae bioreactor was modeled as a window with various concentrations. Meanwhile, Honeybee and Ladybug [40,70], environmental plug-ins for Grasshopper, were used to simulate the energy and lighting performance of the models. Besides, EnergyPlus [55] and OpenStudio [71] engines were used for the energy simulations. Validation of energy simulation results was conducted by case No.600 (BESTest) in the ASHRAE Standard 140–2017 [62]. (See Validation. Section).

For daylight simulation, the software Daysim using the validated Radiance algorithm for annual calculations was used [38]. Daysim as a

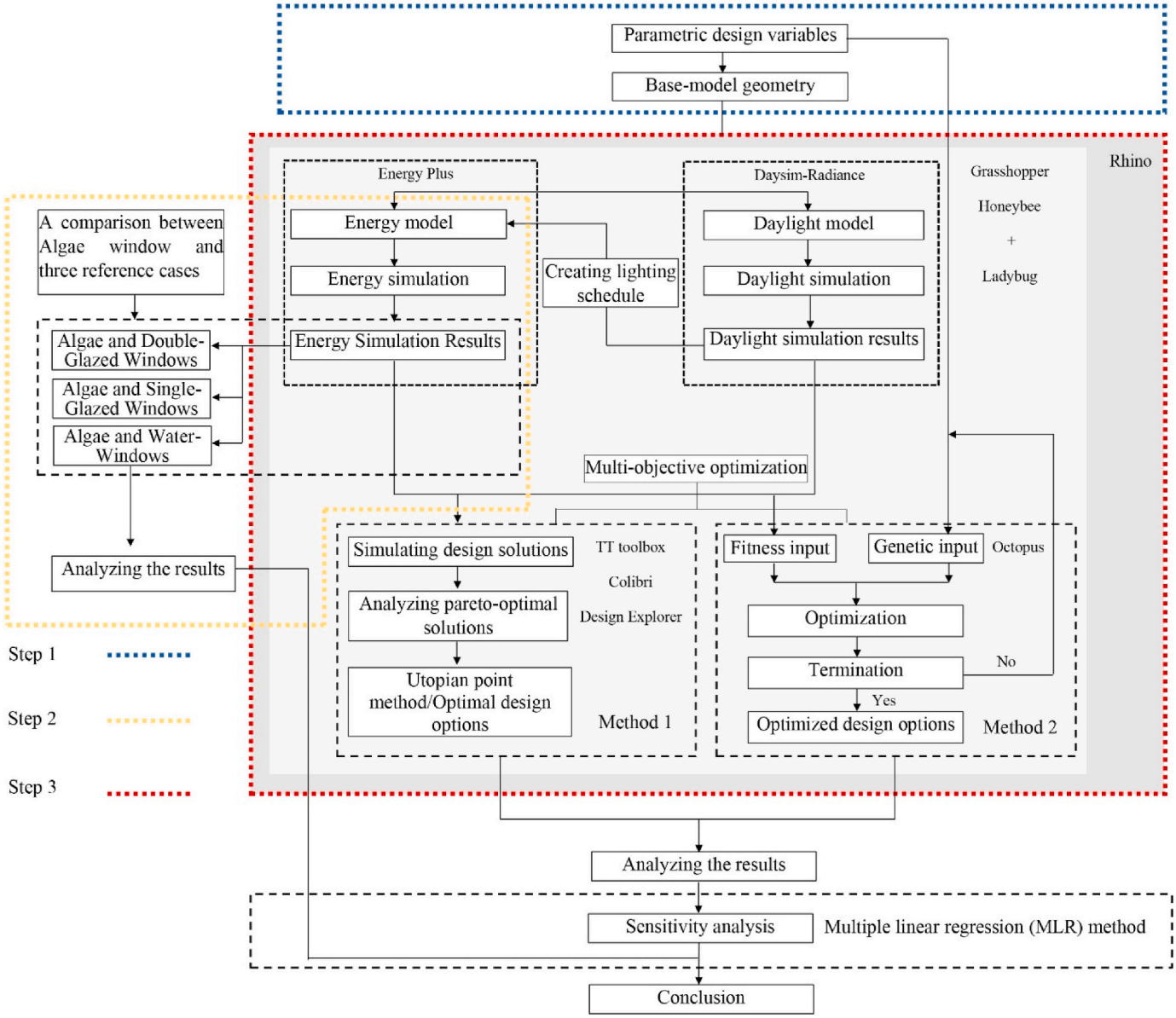


**Fig. 1.** A methodological framework for simulation and optimization of PBR facades.

Radiance-based daylight simulation method uses the concept of the Daylight Coefficient method and the Perez all-weather sky luminance model [72]. In this research, the parametric geometry of the model as well as other inputs including weather files, location of the sensors, and other settings, were connected to the Daylight Simulation component in Honeybee. Using the component Read Annual Result, based on the Daysim, the lighting performance results were then obtained and, as previously mentioned, a lighting schedule was generated to integrate daylighting and artificial lighting. After the simulation, the simulation results file was imported to Grasshopper, by Ladybug reading the daylight performance metrics and generating an annual lighting schedule [40,49]. As the 'idf' file is generated by the energy simulation engine, Ladybug returns the simulation to Grasshopper and provides energy performance metrics.

### 2.1.1. Case study

The case study is a referenced office room based on a typical office building in Mashhad, Iran, consisting of single-zone working space of 4 × 5x3.10 m, located on the middle floor of a multi-story building with no obstructions. The weather data file for Mashhad, Iran, was downloaded from EnergyPlus, onebuilding [73]. Located at the latitude of N 36°17′ 45 and longitude of E 59° 36′ 43 with 985 m elevation above the sea level, Mashhad, Iran, has a cold semi-arid climate based on Köppen climate classification and has a dry climate with little precipitation throughout most of the year. July is the month with the highest average high temperature (34.4 °C) and highest average low temperature (18.7 °C), and January is the month with the lowest average high temperature (7.1 °C) and the lowest average low temperature (−3.8 °C). The climate parameters are summarized in Table 2.

Fig. 2 shows the case-study office space characterized by concrete walls (0.2032 m thick) with thermal insulation (0.049 m thick) and gypsum (0.0127 m thick) on the inner side. The roof construction system is a metal deck (0.0015 m thick) with insulation (0.17 m thick), and the floor includes two Gypsum layers (0.0127 m thick) in addition to attic floor insulation (0.30 m thick). The other materials used in the base model including glazing and their properties are shown in Table 4. The room is surrounded by other office spaces, having adiabatic common walls. Hence, only the façade is diabatic. The studied window is located in the center of each orientation. According to ASHRAE 90.1 recommendations [74], the HVAC system for this building is defined as

**Table 2**
Mashhad climatic parameters, based on EnergyPlus data for Mashhad, Iran [73].

| Weather Data | Unite | Average daily | | Average monthly | |
|---|---|---|---|---|---|
| | | Min | Max | Min | Max |
| Dry-bulb temperature | C | −0.145 | 31.46 | 3.333 | 28.99 |
| Relative humidity | % | 12.33 | 99.62 | 19.83 | 67.22 |
| Dew point temperature | C | −17.96 | 11.92 | −3.59 | 6.92 |
| Wind speed | m/s | 0.62 | 8.16 | 2.005 | 3.76 |
| Direct normal radiation | Wh/m$^2$ | 0.0 | 331.54 | 134.02 | 310.93 |
| Diffuse horizontal radiation | Wh/m$^2$ | 28.45 | 162.62 | 39.07 | 107.65 |
| Global horizontal radiation | Wh/m$^2$ | 36.95 | 346.87 | 93.92 | 330.81 |
| Horizontal infrared radiation | Wh/m$^2$ | 232.12 | 402.79 | 274.64 | 382.89 |
| Total sky cover | tenth | 0 | 10 | 0.53 | 5.98 |
| Barometric pressure | Pa | 89.77420 | 90525.62 | 89989.34 | 90394.53 |

packaged rooftop VAV (Variable air volume) with reheat. The input parameters for the case study are presented in Table 3.

The materials for the base model were defined according to ASHRAE 90.1–2010 recommendation for the studied climate zone. Material characteristics are shown in Table 4. The properties of the window profile, SG-Win, DG-Win, and Water-Win systems adopted for simulation and comparison with the algae window system are presented in Table 4, too.

### 2.1.2. Daylighting and energy modeling

*Simulated window parameters*: The studied parameters in this study are based on the comprehensive literature review to find the variables affecting the thermal and energy performance of the algae bioreactor façade [75]. Among relevant parameters, this study chose to focus on window-to-wall ratio and algae concentrations as two factors that are directly related to algae bioreactor structure and can impact the building-integrated bioreactor's thermal performance. The species of interest in this research is C. Vulgaris due to its high adaptability to severe conditions, such as 10–15% $CO_2$ vol. %, up to 200 and 50 ppm of NO and SO2, respectively [76], high temperature [77], and acidic pH [78].

In this study, two main simulation processes were pursued to achieve research objectives:

1. A parametric simulation was conducted on an existing algae window in the studied office space (Fig. 2). In this step, the energy use of models with the algae window having various concentrations A-10% to A-100% is compared with that of SG-Win, DG-Win, and Water-Win systems. The simulation was conducted for four main building orientations (north, south, east, and west) and 6 different window-to-wall ratios (15%, 30%, 45%, 60%, 75%, 90%), so that we could compare the results with a previous study on the Mediterranean climate [24] that uses the same variables/values. The total number of simulations in this step was 288, which leads to results for all design combinations in four orientations per year.
2. Another parametric simulation was conducted to optimize the parameters of interest and find the optimal solution values based on two desired performance metrics including EUI and UDI. In this step, all possible combinations of 9 window-to-wall ratios (from 10% to 90% at 10% interval), as well as 8 algae concentration levels, were simulated to examine the Pareto front (See optimization section). The total number of simulations for each orientation was 640, leading to 2560 total simulations conducted for all four orientations and all variables of interest.

The thermal characteristics of the algae bioreactor window, as presented in Table 4, are based on Negev et al. [29] that applied an experimental and simulation-based research methodology and determined the algae window U-value, VT, and SHGC for two algae species including Chlamydomonas reinhardtii and Chlorella vulgaris. The algae window's U-value in this research was determined to be 4.9 W/m$^2$K throughout the year, despite small changes in summer and winter. We used 4.9 as the algae window's U-value for the entire year as applying the same U-value for all cases of interest eliminates the impacts of errors from the same source. Additionally, because this study has a

**Table 3**
Input parameters for the research base model.

| Parameters | Value |
|---|---|
| Occupied period | 7–15 |
| Heating and Cooling setpoints | 20 and 26° C |
| Heating and Cooling setback | 15 and 30° C |
| Daylight Illuminance setpoint | 500 Lux |
| Number of people per unit of area | 0.1 ppl/m$^2$ |
| Infiltration rate per area[a] | 0.0003 m$^3$/s-m$^{2a}$ |

[a] According to ASHRAE recommendation for Average building (0.5 cfm/ft2 at 75Pa corresponds to 0.0003 m$^3$/s-m2 at 4Pa).

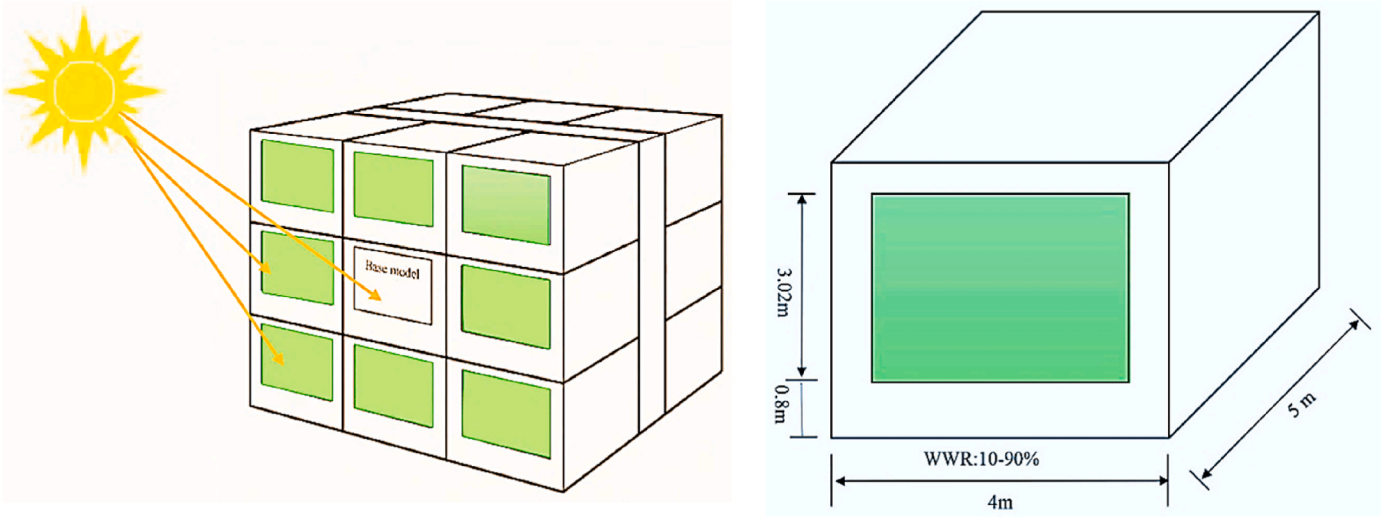


**Fig. 2.** Reference model and the other reference office.

**Table 4**
The input parameters for this case study.

| Construction | | | | U-Value (W/m$^2$K) | R-Value (m$^2$.0 K/W) | Solar Heat Gain Coefficient (SHGC) | Visible Transmittance (VT) |
|---|---|---|---|---|---|---|---|
| Roof | | Total | | 0.28 | 3.53 | - | - |
| | | Roof Membrane | | 16.84 | 0.05 | - | - |
| | | IEAD Roof Insulation R-19.72 IP | | 0.28 | 3.47 | - | - |
| | | Metal Decking | | 30004.00 | 0.00 | - | - |
| Wall | | Total | | 0.77 | 1.28 | - | - |
| | | 1IN Stucco | | 27.34 | 0.03 | - | - |
| | | 8IN CONCRETE HW RefBldg | | 6.45 | 0.15 | - | - |
| | | Mass Wall Insulation R-5.74 IP | | 0.98 | 1.01 | - | - |
| | | 1/2IN Gypsum | | 12.59 | 0.07 | - | - |
| Floor | | Total | | 0.15 | 6.33 | - | - |
| | | 1/2IN Gypsum | | 12.59 | 0.07 | | |
| | | Attic Floor Insulation R-35.07 IP | | 0.16 | 6.17 | | |
| Window | SG-Win | | | 5.80 | – | 0.90 | 0.86 |
| | DG-Win | | | 3.12 | – | 0.81 | 0.76 |
| | Water-Win | | | 4.90 | | 0.69 | 0.79 |
| | Algae Window | Algae-Concentration | 20% | 4.90 | – | 0.40 | 0.45 |
| | | | 30% | 4.90 | – | 0.30 | 0.33 |
| | | | 40% | 4.90 | – | 0.20 | 0.17 |
| | | | 50% | 4.90 | – | 0.16 | 0.14 |
| | | | 60% | 4.90 | – | 0.13 | 0.11 |
| | | | 70% | 4.90 | – | 0.11 | 0.08 |
| | | | 85% | 4.90 | – | 0.09 | 0.06 |
| | | | 100% | 4.90 | – | 0.07 | 0.04 |

comparative objective and, achieving the exact values of energy and daylighting performance metrics is not of interest, variations in algae window's thermal characteristics are not going to impact the results [29]. Umdu et al. [36] in another study determine the U-value of the algae panel through an experiment. Their research, however, aimed to study the effects of design parameters on the thermal conductivity of algae systems. They proposed U-values of 3.84–53.19 W/m$^2$K for algae bioreactors, based on different parameters including air layer, water reservoir, and reservoir wall thickness [36]. Instead of relying on Umdu et al. [36], this research used Negev et al. [29] for thermal properties of the algae window because the latter proposes the algae window characteristics based on various algae concentrations which have considerable impacts on thermal performance. Meanwhile, L. Pagliolico et al. [38] analyzed the potential link between VT values of bioreactor shading screen (PBS) and various sky conditions to explore the relationship between light transmittance changes with different combinations of direct and diffuse solar radiation. The witnessed chaotic behavior of the visible transmittance of PBS and evaluated various VT median values based on various sky conditions. They determined a median value of 0.75 as the reference VT. This mean value is dedicated to PBS without any glazing. In this research PBS regarded as a radiance material while Negev et al. [29] considered algae bioreactor as a window proposing needed parameters for simulation including VT, SHGC and U-value. In the present study the algae bioreactor considered as a window not a mere material, hence the input parameters for simulation tools are different with parameters of a material.

### 2.2. Optimization

In this research, multi-objective optimization was applied. Multi-objective optimization differs from a single objective in complexity, mainly due to the complicated nature of simultaneously meeting several goals that often have competing outcomes [49]. There are two common methods for multi-objective optimization including the weighted sum model and Pareto optimization. The first method assigns different weights to various objectives. The weighted objectives are then summed up to a single cost function. Using this method, the multi-objective optimization problem is turned into a single objective optimization problem. The second method tries to find the Pareto front between each objective [79]. None-dominated or feasible solutions make up Pareto-fronts. To precisely optimize multi-objectives, a set of conditions must be defined to describe the optimal solutions, resulting in Pareto front generation [71,80]. Considering these sets of circumstances, all points known as non-dominated solutions are logically valid and lead to miscellaneous values for the objectives. A multi-objective optimization problem can be expressed mathematically as follow [81]:

Minimize:

$$F(\vec{x}) = [f_1(\vec{x}), f_2(\vec{x}), ..., f_m(x)]^{\mathrm{T}} \quad (1)$$

Subject to

$$g(\vec{x}) \leq 0$$
$$h(\vec{x}) = 0$$

where

$$X_i^{\min} \leq X_i \leq X_i^{\max} (i = 1, 2, ..., n)$$

$$X = [X_1,\ X_2,\ ....X_n]^T \in \Theta$$

$$Y = [Y_1,\ Y_2,\ ...,\ Y_n]^T \in \Psi$$

Here $m$ indicates the number of objective functions which is two in the case of the present study, Θ is the search space with $n$ dimensions which is recognized as upper and low bounds of the decision variable $xi$ ($i = 1, 2, ..,n$).

$$X^{\max} = X_1^{\max},\ X_2^{\max},\ ....X_n^{\max}]^T \quad (2)$$

$$X^{\min} = X_1^{\min},\ X_2^{\min},\ ....X_n^{\min}]^T \quad (3)$$

Ψ is the $m$-dimensional vector space of objective functions and is defined by Θ and the objective function f(x). $g_j$ (x) 0 (j = 1, 2, ..,$p$) and h(x) = 0 (j = 1, 2, ..,$q$) denotes $p$ and $q$ being the number of inequality and equality constraints, respectively. If both $p$ and $q$ are equal to zero then the problem is simplified as an unconstrained optimization problem.

In the present study, the multi-objective optimization technique was applied to find design options with minimum energy use intensity and maximum useful daylight illuminance (Equation (4)).

$$E_{\text{total}} = (E_H + E_C + E_L + E_E) \quad (4)$$

$$EUI = E_{\text{total}} / \text{Gross floor area}$$

Where $E_H$ indicates basic demand for heating energy, $E_C$ for cooling, $E_L$ + for lighting, and $E_E$ for electrical equipment, respectively. Since

daylight and artificial lighting are regarded as important factors having a great impact on building energy consumption, they should be considered in building simulation. Also, solar radiation influences the cooling and heating loads of the building, hence multi-objective optimization was applied to enhance the optimal solution for the two objectives EUI and UDI.

$F(x_1) = \min$ (EUI)

$F(x_2) = \max$ (UDI)

The algorithm based on dimensions and features of the algae window was identified. The parameters applied in this research are window to wall ratio and algae window concentration resulting in different window characteristics including VT and SHGC. The parameters including algae window to wall ratio and algae concentration range from 10% to 90%, and 10%–100% density at 10% interval (Table 4), respectively.

Pareto-front is used to find optimal solutions. Hence, by recognizing the Pareto solutions considering the best EUI and UDI as well as the balanced options, the best optimal solution variable values were recommended (Fig. 11). The best Pareto front solutions can be achieved by applying the Utopian point method assuming that there is a Utopian point, and the Pareto front points have the minimum Euclidean distances from the Utopian point. The optimal value can be defined [64] by finding the shortest Euclidean distance using equation (5).

$$d_E = \min \sqrt{\left(Q_1 - Q_1^*/Q_1 norm\right)^2 + \left(Q_2 - Q_2^*/Q_2 norm\right)^2} \quad (5)$$

where $Q_1^*$ and $Q_2^*$ are the coordinates for the Utopia point of the objective function F ($\times_1$) whose minimum value is desirable, and objective function F ($\times_2$) which demands maximum values. Besides, $Q_1$ and $Q_2$ are the point coordinates on the Pareto optimal front. $Q_1$ norm and $Q_2$ norm are regarded as normalization point coordinates in the problem areas. $Q_1$ norm and $Q_2$ norm are defined based on the minimum value of $Q_1$, and the minimum value of $Q_2$, respectively.

At the beginning of the optimization design process, evolutionary algorithms [82], were first considered to be applied to achieve multi-objective optimization. However, since this method may omit some solutions through creating new generations and suggests only some of the possible optimal solutions and not illustrates the trends of the optimal results, after conducting an optimization process and analyzing the results for one orientation, it was decided not to apply the computational plugins which are based on evolutionary algorithms in the first step. Since, this research aims to optimize design parameters for each orientation of the building separately, to comprehensively evaluate the impact of parameters on performance metrics, and observe the result trends for 640 design option in each orientation, it was decided to pursue the process of simulating possible solutions and not omit some options to reach the optimum design options and visualize and analyze the results by Design explorer [83], then applying Utopian point method. On the other hand, evaluating all possible design options for each orientation and all building aspects is a time-consuming process. Therefore, tools in Grasshopper which are vastly applied for Performance-based parametric design were used. By applying the TT toolbox and its tool Colibri [84] possible solutions were simulated. Since modeling and computing the design options are a laborious process, using the tools was a practical help to achieve this aim. Design parameters were connected to the Colibri Iterator component and the performance metric was connected to the Colibri Parameters. Then both component outputs were connected to the Colibri Aggregator component. Parameters were considered as Genome and UDI and EUI were linked to Phenome. Through its tools, the TT toolbox automatically saves all possible solutions and their features, and the Design explorer visualizes design solutions. Hence, by selecting each option, all related information is accessible. Providing visualization and filtering group of iteration-sets of design solutions that are both intimately related and potentially scattered across a vast, high-dimensional possibility space, Design Explorer is tool for exploring design spaces on the web. The results of this part are illustrated in Figs. 6–9, and the range of optimum solutions achieved by using the Utopian point method is evaluated based on algae density and window to wall ratio.

In the second step, Octopus a Grasshopper plugin used for multi-objective optimization to enhance the methodology and evaluate the results and complete the first run of optimization. Octopus is based on Pareto Evolutionary Algorithm (SPEA-2) in combination with the Hypervolume Estimation Algorithm (HypE) [85,86] used in this study, to achieve multi-objective optimization. Being deployed in most recent multi-objective evolutionary algorithms, the contributing hypervolume is one of the most popular second-level sorting criteria due to its attractive theoretical properties. The hypervolume measure or *S*-metric of a population A is the volume of the union of regions of the objective space which are dominated by A and bounded by some appropriately chosen reference point $\overrightarrow{R} \in R^m$, that is [87],

$$HYP(A) := VOL(\cup_{\alpha \in A}[f_1(\alpha), r_1] \times \ldots \times [f_m(\alpha), r_m]) \quad (6)$$

By using the hypervolume as a second-level sorting criterion for comparing incomparable individuals, the respective contribution of each individual to the total hypervolume is measured. The contributing hypervolume of an individual $\alpha \in A$ is given by

$$\text{CON}(\alpha, A) := \text{HYP}(A) - \text{HYP}(A \backslash \{\alpha\}) \quad (7)$$

Besides, being applied to problems with arbitrary numbers of objective functions, HypE as a novel hypervolume-based multi-objective evolutionary algorithm incorporates a new fitness assignment scheme based on the Lebesgue measure, where this measure can be both exactly calculated and estimated employing Monte Carlo sampling. Monte Carlo methods can be considered as a collection of computational techniques for the (usually approximate) solution of mathematical problems making fundamental use of random samples. Integration and optimization are two classes of statistical problems which are most commonly addressed within this framework [88,89]. According to Everson et al. [90], the Monte Carlo algorithm can compare two nondominated sets *X* and *X′* by calculating the fraction of space dominated by *X* and not by *X′*, and vice versa. This can be done by normalizing all objectives onto the range [0 … 1] then randomly generating points in the unit hypercube and testing each point to understand whether it is dominated by *X* and/or *X′*. This algorithm has complexity *O(nmN)* in the worst case, where *N* is the number of samples used, and this complexity can be reduced by using a more advanced data structure to store the points. The error induced by the random sampling decreases as $\sqrt{N}$, and it is independent of *n* [91].

Hence, Monte Carlo approximation, in brief, as a technique obtaining random configuration for the variable of interest can be defined mathematically with the following formula [92,93]:

$$E_X \approx 1/N \sum_{n=1}^{N} x_n \quad (8)$$

Where *X* refers to random variables, while *x* is for the random elements making that population. All *x*'s can be regarded as the possible outcomes of the random variable *X*. The approximation of the average value of *X* as the random variable is equal to the sum of the sample size *N* chosen from the population divided by the sample size.

Octopus plugin is getting popular especially in the field of multi-objective optimization of building performance design [40,49,94] and verified by recent research [95,96]. Parameters including WWR and algae density were connected to the Genetic input, while performance metrics, EUI, and UDI were connected to the Fitness input (Fig. 1). In the present study, according to the possible design options population size of the first generation was considered 50, meaning that 50 design solutions were selected from all candidate options, randomly. The population size of all the further generations was 20 according to the number of possible


**Fig. 3.** Energy use differences (kWh/m$^2$/y) in the case of algae window from the reference single-glazed window (SG-Win), based on variations in algae concentration and window-to-wall ratios in four orientations. Each diagram in the Figure shows 8 groups of 6 bars. Bars with unique colors represent window to wall ratios, and each of the 8 bar groups represents a certain algae density percentage.

design solutions. There are various criteria for terminating the process. The first is meeting the number of generations defined by the user, the second is time simulation defined by the user too, and the third is manually stopping the process when the user decides that the result is satisfactory [40,97]. The termination criterion in this study was defined by users which continued to 15 generations.

Applying principal in nature including selection, crossover, and mutation, the Octopus improves the population of solutions [40]. Elitism, Mutation probability, Mutation rate, and Crossover rate are defined as 0.5, 0.2,0.9, and 0.8 respectively, and sequentially in the present study. Blend Crossover Algorithm [98] an operator for crossover, includes the following steps [99]:

1. Select two parents $X^{(t)}$ and $Y^{(t)}$ from the parent pool
2. Create two offspring $x^{(t+1)}$, and $y^{(t+1)}$ as follows:
3. For i = 1 to $n$ do
4. $\Delta = 0.2$
5. Choose a uniform random real number $\alpha \in \langle -\Delta, 1+\Delta \rangle$
6. $x_i^{(t+1)} = (\alpha_i \times X_i^{(t)}) + ((1-\alpha_i) \times Y_i^{(t)})$
7. $y_i^{(t+1)} = (\alpha_i \times Y_i^{(t)}) + ((1-\alpha_i) \times X_i^{(t)})$
8. End do

The steps of the Point Mutation algorithm [100] for mutation are as follows (Δ refers to the parents' attribute range):

1. Select one parent $X^{(t)}$ from the parent pool
2. Create one parent $x^{(t+1)}$ as follows:
3. Choose an integer random real number $u \in 0, n-1$
4. Sigma = $\Delta/10$
5. Choose a Gaussian random real number $g \in 0, 1$
6. $x^{(t+1)} = X_u^{(t)} + (sigma \times g)$

Comparing with other similar optimization tools in Grasshopper, Octopus has advantages including having the ability to define multiple objectives that can be evaluated simultaneously, which provides optimal solutions, presenting the best mode of objectives. This method provides the potential for examination of correlations between different objectives as well as a more comprehensive arrangement of outcomes compared to single-objective optimization analysis [94]. After several iterations, while removing the unfit solutions, the results which are optimized design alternatives meeting the objective function sets are yield. The comparison between the results of the two methods is illustrated in Table 9. The main objective of the optimization process in this research is to identify the optimum design solutions for integrating bioreactor technologies with the building facade for all four main building orientations in the BSk climate to meet designers', architects', and engineers' needs in the early design stage of building. When integrating microalgae bioreactors in façade systems, it should be noted that microalgae have three major techniques of culturing: batch, continuous,

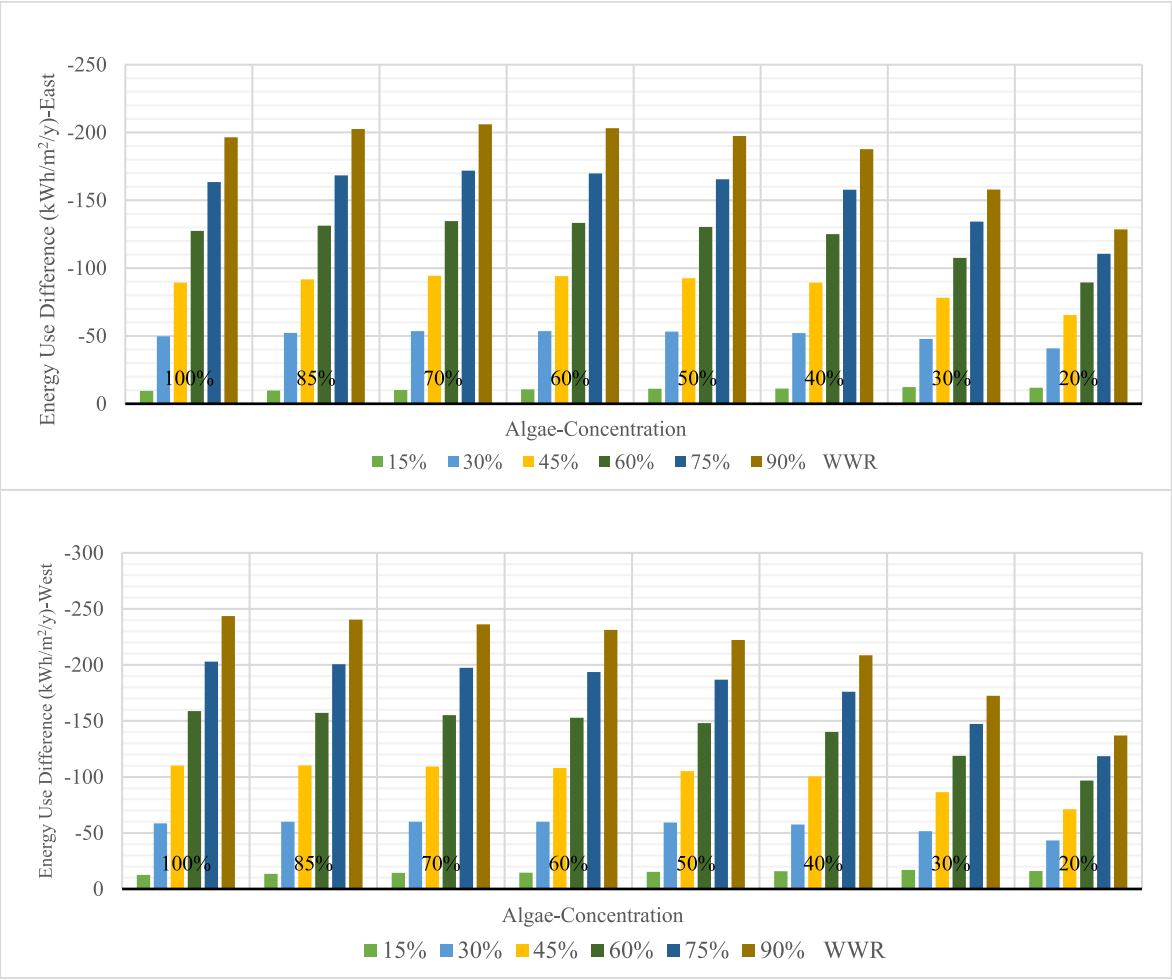


**Fig. 3.** (*continued*).

and semi-continuous [101]. In the batch technique, the algae are harvested after inoculating the cells into a container of fertilizer and growing them to reach their maximum density. Hence, the bioreactor is filled with algae which are later emptied after the algae reach their highest density, and this cycle continues. In the continuous technique, it is possible to keep the medium density constant even during the year to reach an efficient culture density for various purposes. In this system, a certain amount of microalgal culture solution will be harvested intermittently while the same amount of medium is refilled [102,103]. Hence, the growth environment of the cells in the reactor remains constant. In this technique, microalgae are harvested and, in the meanwhile, new microalgae are injected into the bioreactor. The continuous system is the technique that can best be applied in building-integrated bioreactors as the shape of algae culture density has the potential to be integrated with the building façade [8,104]. Hence, the algae medium density is controllable based on desired parameters. In this study, the algae density is considered as an independent variable for optimization, and its effects on performance metrics are examined with the aim to provide an energy-efficient building solution with sufficient daylight since the algae impact both thermal and shading properties of the window [14,29,105]. In other words, algae density is optimized for building performance metrics only, and algae density optimization for biomass production is not included in the scope of research. This ofcourse would be an interesting topic to be studied by future research. The main drawback of the batch culturing system for building applications, as compared with the continuous system, is that it cannot reach the steady-state conditions [103]. This is because the condition in which microalgae culture spends its natural growth period to reach the highest density is not always favorable for building energy efficiency, as the culture density cannot be adapted with the needed amount of sunlight penetrating indoors. For example, consider the warmest period of the year that the building demands windows with high shading and thermal insulation performance. In the batch culture, when algae reach the high density, it should be harvested and replaced with a low-density medium, which for a while cannot block sunlight from entering indoors until it reaches acceptable density. This in turn increases building cooling loads in the warmest parts of the year. Accordingly, this research uses the continuous culture technique to propose optimal solutions based on two variables including algae density and WWR to minimize EUI and maximize UDI.

## 3. Results and discussion

The results are analyzed in two main categories: first, energy simulation results of microalgae window-based building model to be compared with that of SG-Win, DG- Win, and Water-Win systems based on WWR and algae density variations at four main orientations; second, optimization results.

### 3.1. Simulation

The simulation was conducted based on 8 different algae densities with their specific thermal characteristics and 6 various window-to-wall ratios at four main orientations. Figs. 3–5 illustrate the changes in

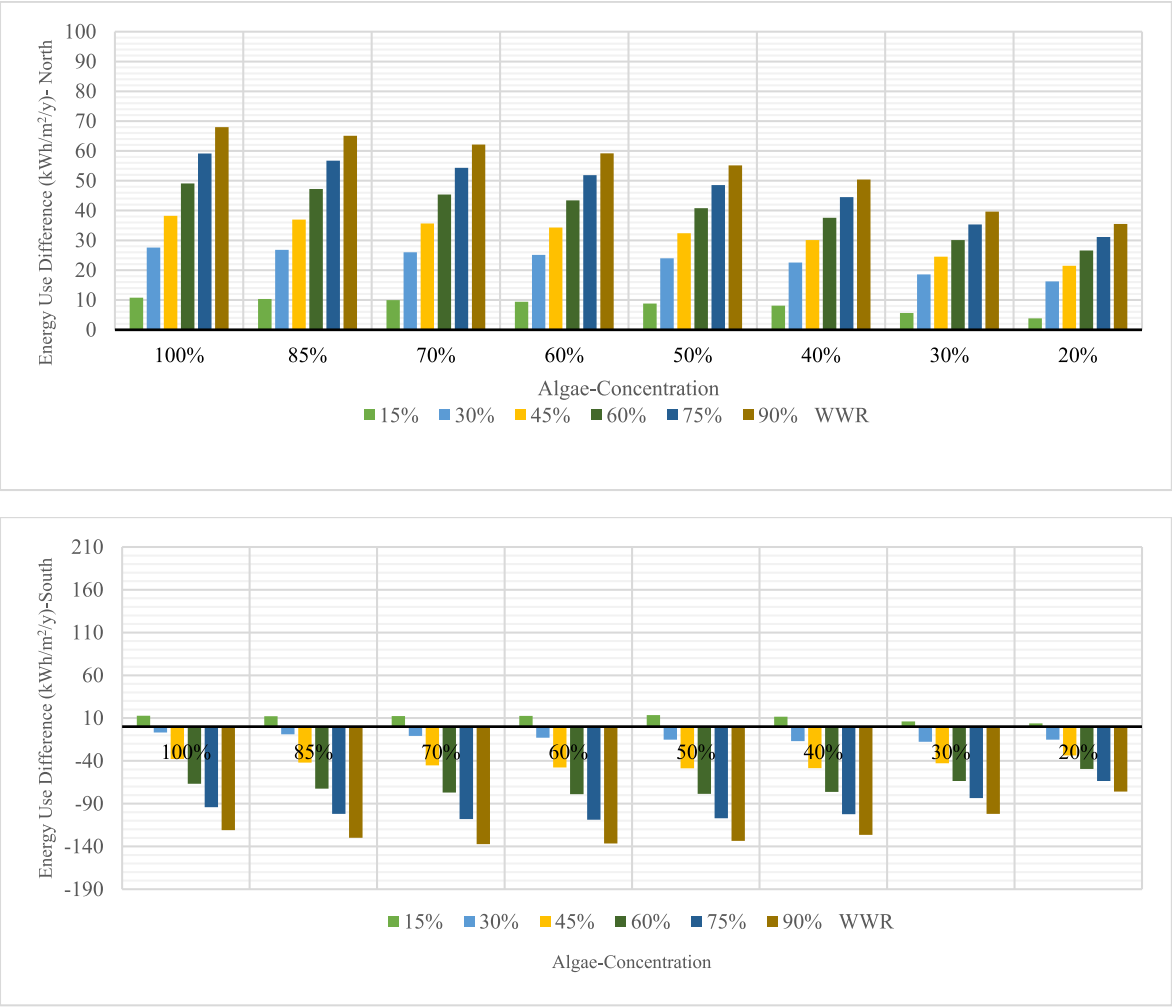


**Fig. 4.** Energy use differences (kWh/m$^2$/y) in the case of algae window, from the reference double-glazed window (DG-Win), based on variations in algae concentration and window-to-wall ratios in four orientations. Each diagram in the Figure shows 8 groups of 6 bars. Bars with unique colors represent window to wall ratios, and each of the 8 bar groups represents a certain algae density percentage.

energy consumption of the studied model containing the algae window, as compared with models with double-glazed window (DG-Win), single-glazed window (SG-Win), and water window (Water-Win) in four main building orientations. The results show that the potential energy saving is different based on algae density, window to wall ratio, and façade orientation (Also see Tables A1, A2, and A3 in appendix). Figs. 3–5 were determined as energy use differences between the algae window and the reference models with SG-Win, DG-Win, and Water-Win systems. Figs. 3–5 each consists of four diagrams representing north, south, east, and west orientations. Each diagram in Figs. 3–5 shows 8 groups of 6 bars. Bars with unique colors represent window to wall ratios, and each of the 8 bar groups represents a certain algae density percentage. The results demonstrate that compared to the south, east and west orientations, the north-facing algae window performs differently in terms of energy-saving, meaning that this is the only orientation that does not lead to energy saving except when algae density is 20% and 30% and WWR is not 30% based on the SG-Win reference case. Limited energy-saving opportunities in the case of a north-facing algae window occur mainly because there is minimal direct solar radiation in the north results in more thermal effect by U-value than VT and SHGC. Conversely, in the south, east, and west, radiation transmittance and shading have more impact on energy consumption than thermal effect. In the meanwhile, except for the case of the model with a north-facing algae window in which finding a general energy-saving pattern across different variables is a challenge, the increase in the window-to-wall ratio of algae window leads to more energy savings in all other orientations, with 90% WWR leading to greatest energy savings. The greatest energy saving potentials among all possible design solutions occur in the model with a west-facing algae window with 100% algae concentration, and 90% WWR which leads to 243.55, 164.65, and 183.16 kW h/m$^2$/y of energy savings, compared with reference models using SG-Win, DG- Win, and Water-Win systems, respectively. In the south and east orientations, the greatest energy savings occur in the algae window with 70% algae density and 90% WWR, which leads to 179.08 and 205.99 kW h/m$^2$/y of energy savings, respectively, compared with the single-glazed reference model. In the north, the highest energy saving potential occurs in algae window with 90% WWR and 20% algae density, leading to 18.66 kW h/m$^2$/y of energy savings, compared with the single-glazed reference model. Table 5 provides further details for comparison of algae window, SG-Win, DG-Win as well as Water-Win by listing percentile and maximum energy use differences. In general, the highest energy saving percentages are achieved by using algae windows in the south (algae density of 70% and WWR of 90%), with a maximum energy use improvement of 53.74% over the SG-Win reference model. This improvement significantly drops when comparing algae window with a double-glazed window and water window reference models.

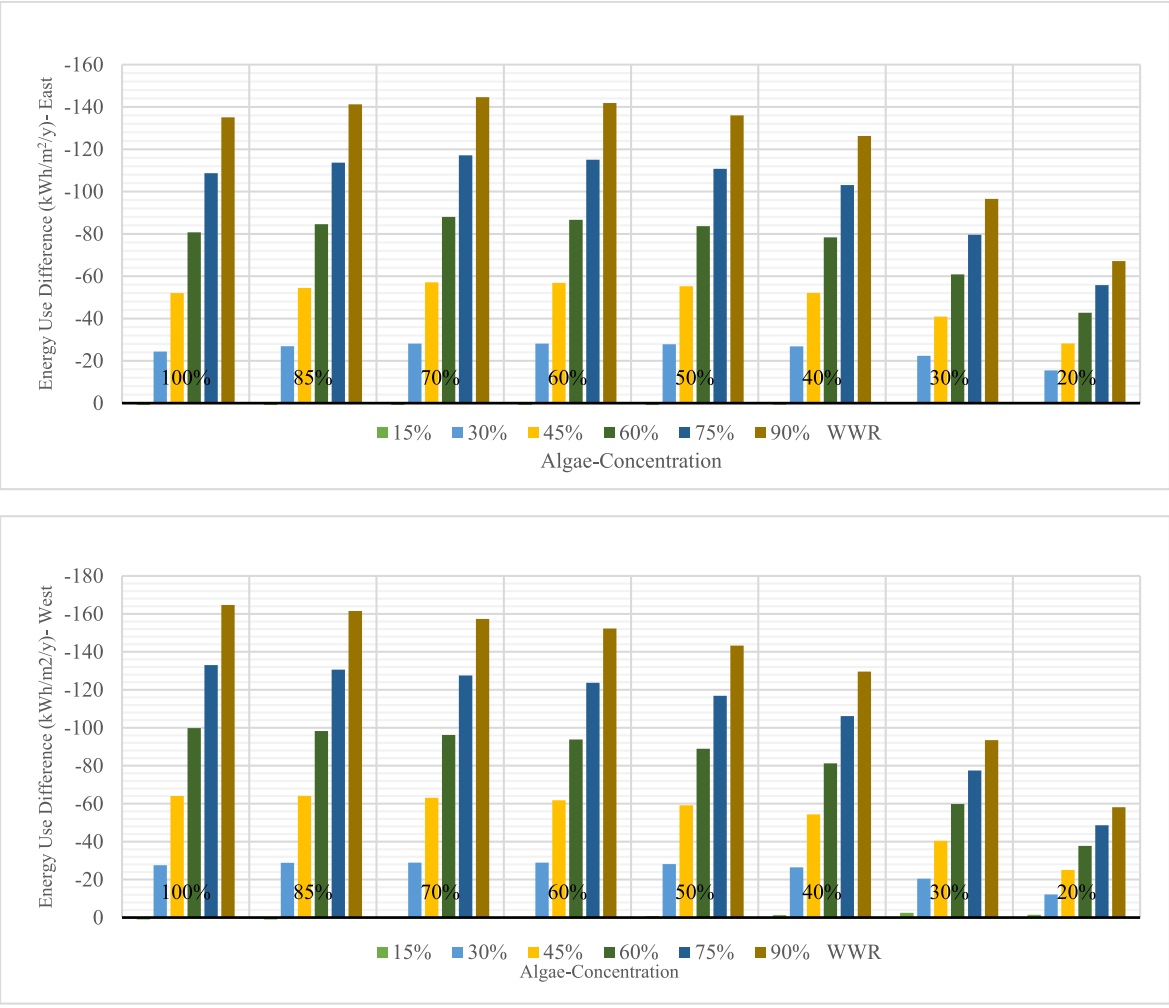


**Fig. 4.** (*continued*).

The simulation results in this step confirm the results reported by Negev et al. [29] for algae windows containing C. vulgaris species in the Mediterranean climate. The results in both climate zones demonstrate a similar trend, even though the exact values are different. Negev et al. [29] similarly report the performance of algae windows in the north orientation being different as compared with other orientations, as no energy savings are reported in this orientation for different algae densities and window-to-wall rations, as compared with SG-Win, DG-Win, and Water-Win reference models. Besides, as Negev et al. [29] report for the south, east, and west orientations, the greater the window-to-wall ratio, the more energy-saving is provided, generally. Besides, despite Negev et al. [29] that reports no energy saving for the PBR algae windows of less than 30% WWR at any of the four main orientations in the Mediterranean climate zone, we found potential energy savings in algae windows of less than 30% WWR in the cold BSk climate. In the Mediterranean climate, Negev et al. [29] report the greatest energy use differences to occur in south orientation, followed by the west, while in the cold semi-arid climate the maximum energy use difference was found to occur in the west, while the highest energy saving in percentage happens in the south. Consequently, in terms of the percentages of energy-saving, south, west, and east stand at the first, second, and third place, respectively, in both climate zones, while the algae window in the north leads to no energy savings in the Mediterranean climate and the least energy-saving (10.18%) in BSk climate, comparing with the SG-Win reference model (Table 6).

### 3.2. Scatterplots of optimization results

In the optimization process, the energy use intensity and useful daylight illuminances were evaluated based on various algae culture densities and window-to-wall ratios for different building orientations, using all possible design solutions. Accordingly, scatterplots were developed based on 2560 simulation results in the optimization data collection process. Figs. 6–9 illustrate the optimization results including scatter plots of two performance metrics; energy use intensity and useful daylight illuminance. In these figures, the colors represent various algae densities for the algae window integrated into different building orientations. Scatterplots illustrate all possible design options as well as the optimal ones defined by the Pareto frontiers. According to the optimization objective of achieving minimum EUI and maximum UDI, the optimal design solutions tend to occur in the top-left corner of the graphs in Fig. 6–9. As shown in Figures, scatterplots have negative and positive correlations as shown by the trends. In other words, some design options that have optimum EUI are associated with unfavorable percentages of UDI and vice versa. Meanwhile, the optimum options on the upper-left of the graphs in Figs. 6–9 include non-dominated solutions that surpass other solutions in terms of minimum EUI and maximum UDI at the same time and there are no better solutions for the two main performance metrics than these Pareto optimums. In the optimization step of this research, the best design options for each of the four main orientations were selected in terms of best EUI, best UDI, and the balanced options in between. Due to the sharp shape of the Pareto front in the east and west, it can be concluded that the relationship between the two

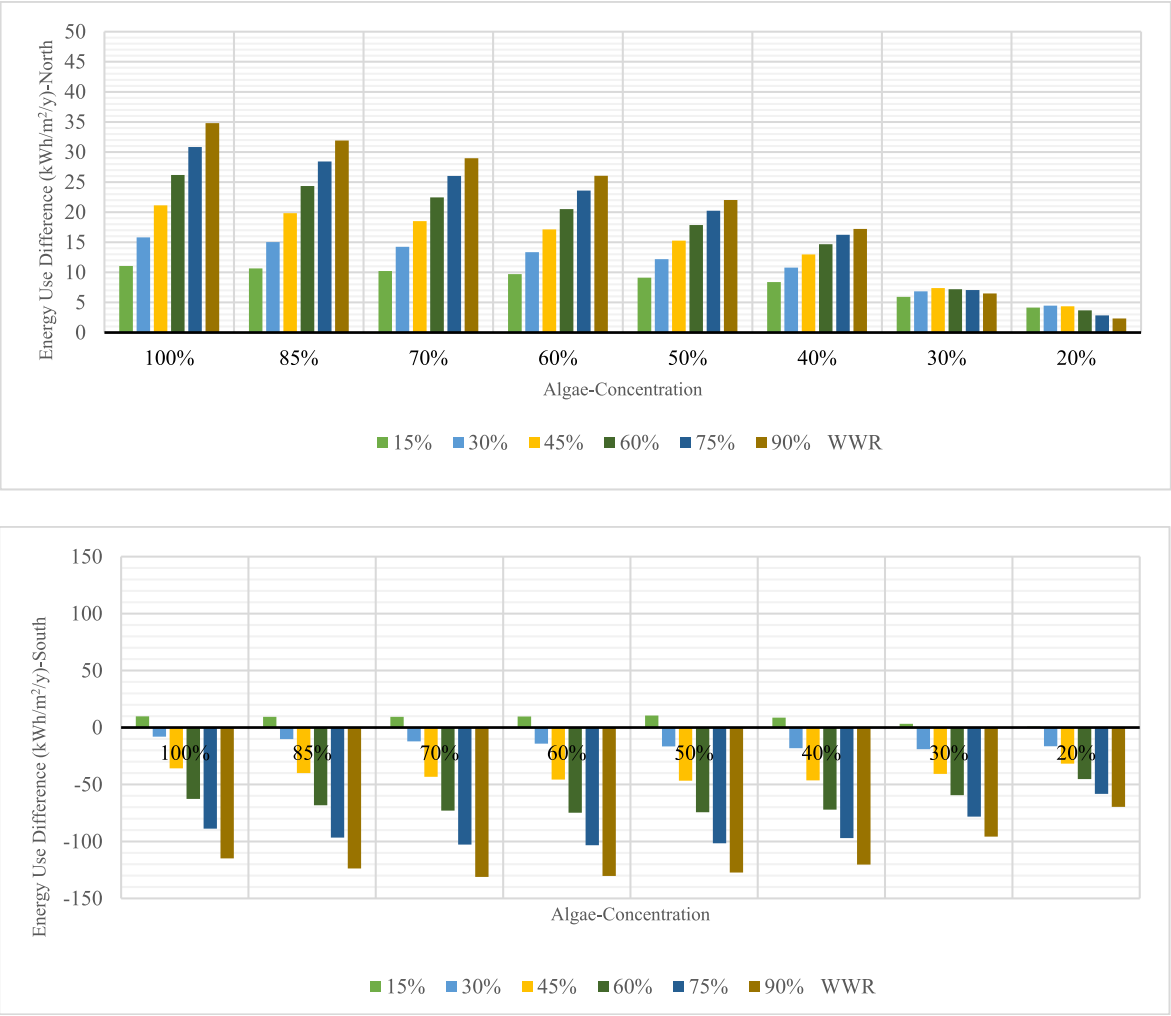


**Fig. 5.** Energy use differences (kWh/$m^2$/y) in the case of algae window, from the reference water windows (Water-Win), based on variations in algae concentration and window-to-wall ratios in four orientations. Each diagram in the Figure shows 8 groups of 6 bars. Bars with unique colors represent window to wall ratios, and each of the 8 bar groups represents a certain algae density percentage.

objectives is stronger in these two orientations than in the north and south where there is a curved shape.

### 3.3. Optimization results

Fig. 10 illustrates three optimal design options including best UDI, best EUI, and a randomly selected balanced option, created by the parametric model for different orientations. The numerical values for each option are listed below the option in Fig. 10 and the percentages of UDI are shown as a color block at each sensor location in the building work plane. Accordingly, the highest EUI value is about 75–112 kW h/$m^2$/y and the highest UDI value is between 78% and 91%. Table 7 demonstrates the minimum and maximum EUI and UDI values for each orientation as well as the total average values of the two performance indices based on the window-to-wall ratio and algae density. According to this table, the highest total average EUI in south, east and west orientations occurs in the algae window with the low density (20%) and is 131.78, 185.79, and 205.00 kW h/$m^2$/y, respectively, while in the north, the highest average EUI value occurs in 100% algae medium with 143.31 kW h/m2/y. Besides, the lowest total average EUI in the south, east, and west occurs in algae densities of 60%, 70%, and 100%, respectively. In general, the lowest total average EUI value, considering all algae density percentages, occurs in the south with 117.20 kW h/$m^2$/y, while the west leads to the highest average EUI value of 171.22 kW h/$m^2$/y. Meanwhile, an algae window in the north could enjoy the maximum average UDI of 85.27%, whereas the minimum average UDI occurs in the south with 70.33%. According to Table 9, the results of the optimization process using the Octopus plugin as the second method falls within the range of the first method as mentioned above. However, a few points fall out of the range. Besides, the number of Pareto solutions is limited in the second method. This is justifiable, since considering the history of Octopus Pareto front, the number of points is fewer than that of the first method. This is due to fact that evolutionary algorithms provide a randomly selected population for the first generation and the other generations are based on the selection, mutation, and crossover between the first options. Hence, the number of options evaluated may be more limited than the situation considering all options.

#### 3.3.1. Optimum solutions

Fig. 11 illustrates the design solutions with optimum EUI and UDI, and the balanced options, clustered for each building orientation and shows related window size and algae density. The main results, according to Fig. 11, are summarized as follows:

1. In the north, the highest UDI happens in the design option with 38% WWR and the minimum EUI occurs in the option with 10% WWR,


**Fig. 5.** (*continued*).

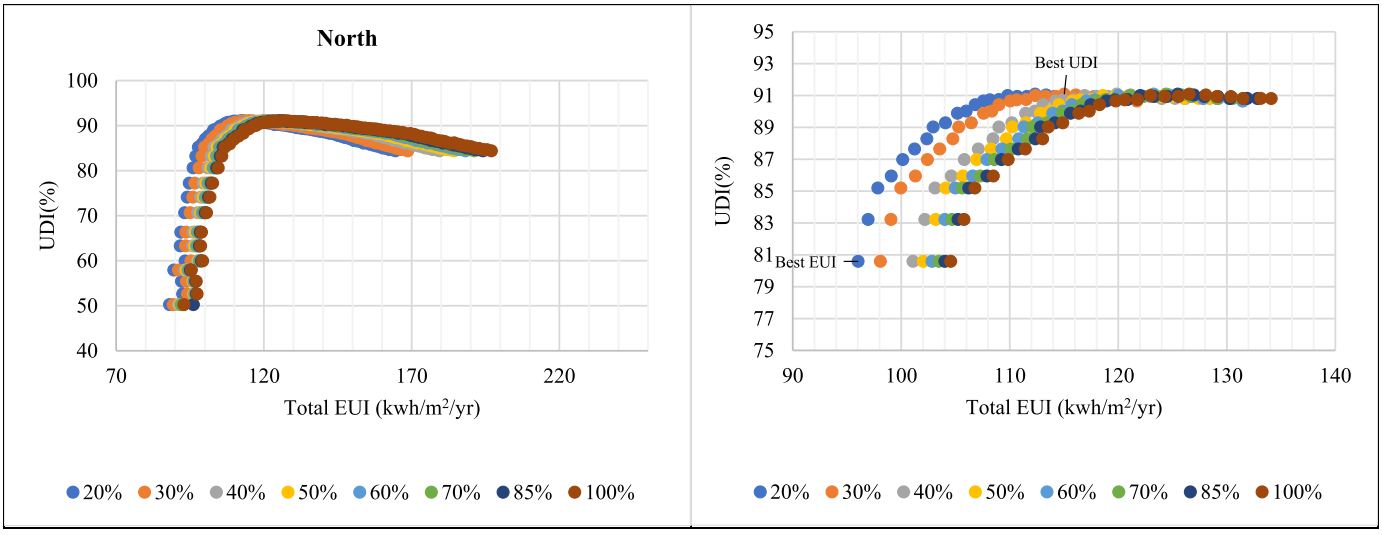


**Fig. 6.** Scatterplots showing the performance of EUI against UDI and Pareto fronts for north orientations.

across all algae densities (Table 7, Fig. 11). The optimum solutions to simultaneously provide the maximum possible EUI while keeping a minimum UDI occur in options with 20%, 30%, and 40% algae densities. The optimum solutions for north orientation include a window with 20% algae density, and 20–29% to 30–38% WWR, a window with 30% algae density and 31–37% WWR, and a window with 40% algae density and 33% WWR.

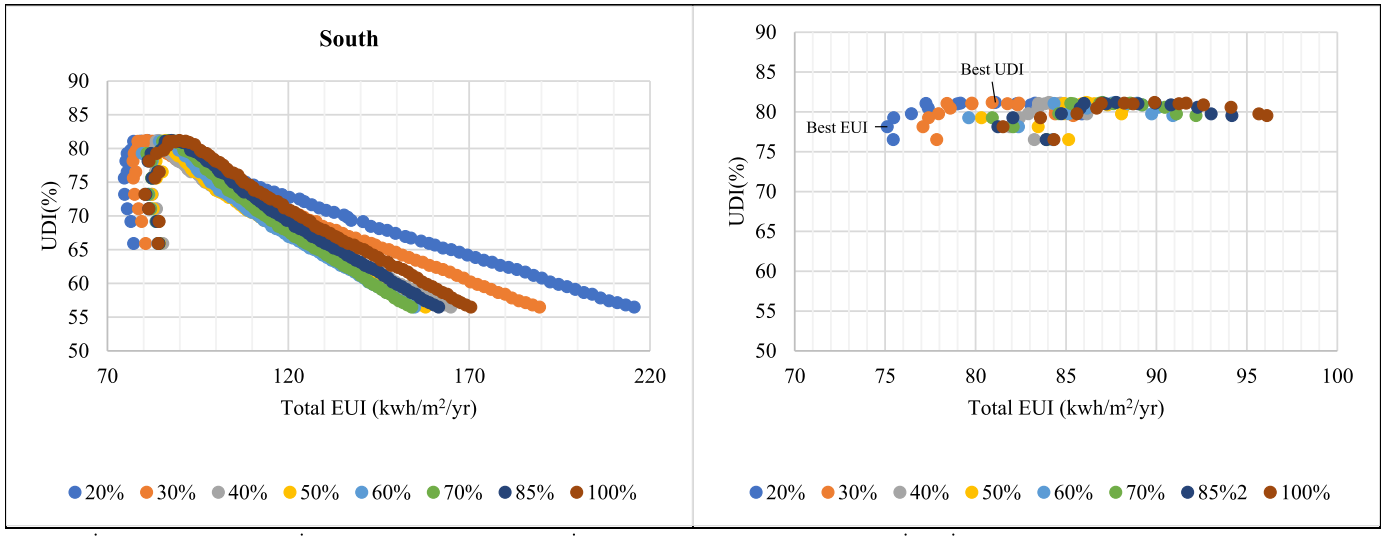


**Fig. 7.** Scatterplots showing the performance of EUI against UDI and Pareto fronts for south orientation.

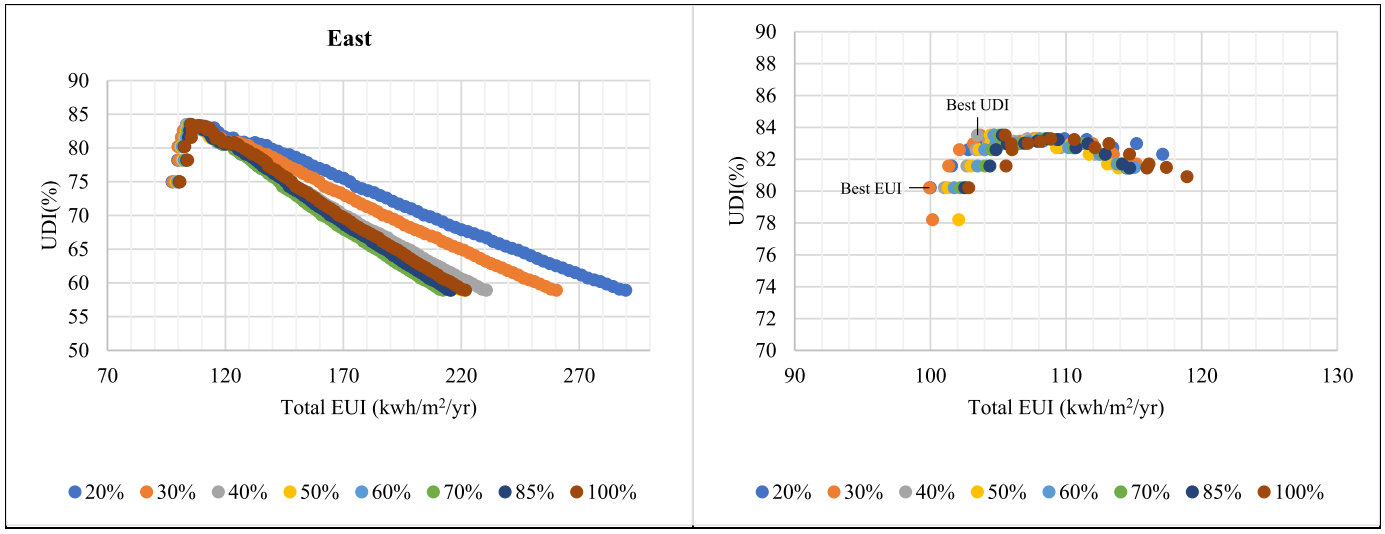


**Fig. 8.** Scatterplots showing the performance of EUI against UDI and Pareto fronts for east orientation.

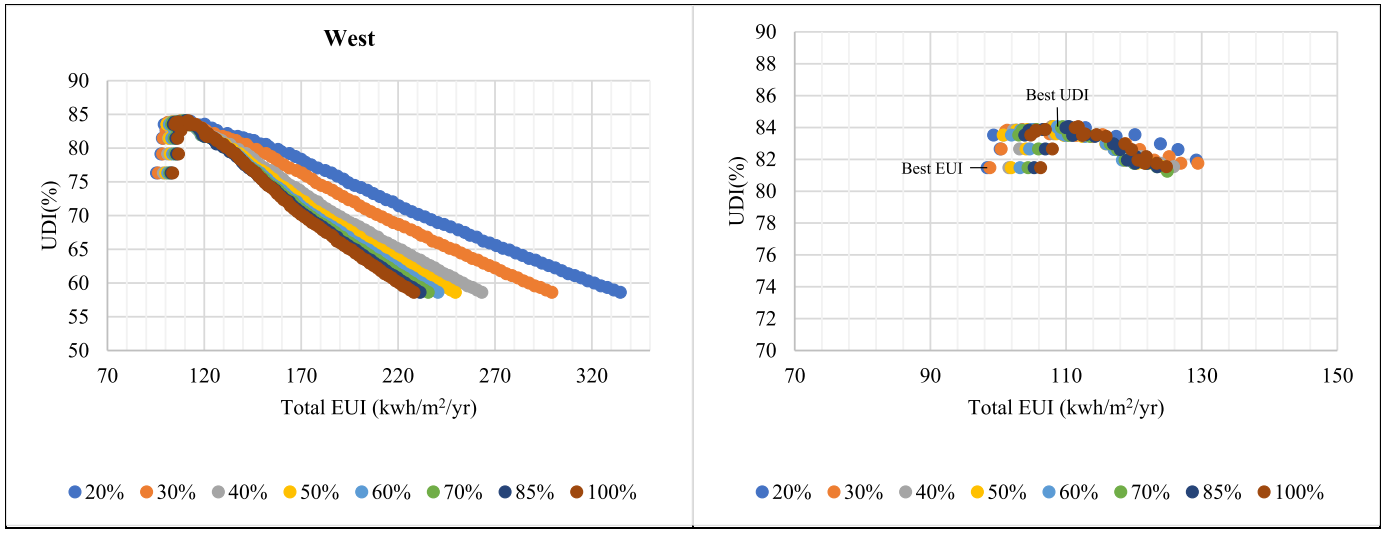


**Fig. 9.** Scatterplots showing the performance of EUI against UDI and Pareto fronts for west orientation.

**Table 5**
Fractional impact of maximum energy use differences of the algae window compared to three reference cases at all façade orientations.

| Orientation | Energy use (kWh/m$^2$/y) | | Max. Energy use differences from SG-Win | | | Energy use (kWh/m$^2$/y) | | Max. Energy use differences from DG-Win | | | Energy use (kWh/m$^2$/y) | | Max. Energy use differences from Water-Win | | |
|---|---|---|---|---|---|---|---|---|---|---|---|---|---|---|---|
| | Algae-Win | SG-WIN | Size[a] | Energy use difference | Fractional impact | Algae-Win | DG-WIN | Size | Energy use difference | Fractional impact | Algae-Win | Water-WIN | Size | Energy use difference | Fractional impact |
| North | 164.561 | 183.227 | W-90% D-20% | −18.666 | 10.18% | 197.026 | 129.064 | W-90% D-100% | 67.961 | 52.65% | 197.026 | 162.217 | W-90% D-100% | 34.80 | 21.45% |
| South | 154.157 | 333.242 | W-90% D-70% | −179.085 | 53.74% | 154.157 | 291.4902 | W-90% D-70% | −137.333 | 47.11% | 154.157 | 285.255 | W-90% D-70% | −131.09 | 45.95% |
| East | 212.284 | 418.28 | W-90% D-70% | −205.996 | 49.24% | 212.284 | 356.925 | W-90% D-70% | −144.64 | 40.52% | 212.284 | 362.92 | W-90% D-70% | −150.63 | 41.50% |
| West | 228.203 | 471.762 | W-90% D-100% | −243.559 | 51.62% | 228.203 | 392.859 | W-90% D-100% | −164.656 | 41.91 | 228.203 | 411.366 | W-90% D-100% | −183.163 | 44.52% |

(−) = Saving.
(+) = Non saving.
[a] Size: D = Density, W=WWR.

2. In the south, 23% WWR leads to an optimum UDI in all algae densities. In this orientation, the optimum EUI occurs window with 14% WWR and 20% algae density (Table 7, Fig. 11). However, considering both EUI and UDI performance metrics through multi-objective optimization, only 20% and 30% algae densities lead to optimum solutions. The optimum solutions in the south include the use of a window with 20% algae density and 16–23% WWR, and a window with 30% algae density and 19–21% and 23% WWR.
3. In the east, similar to the north, the optimum solutions are defined within a 20–40% algae density range. Besides, the favorable window-to-wall ratios for optimum EUI and UDI are 10% and 16%, respectively. The optimum design options for an algae window integrated with the east facade include a window with 20% algae density and 12–14% WWR, a window with 30% algae density and 13–16% WWR, and a window with 40% algae density and 16% WWR.
4. In the west, contrary to the other orientations, the optimum solutions are not limited to specific density percentages and can occur in any algae density. Therefore, the optimum solutions in the west include algae windows of any algae density but with 12–18% WWR. Correspondingly, the window with 20% and 50% algae medium have a 14–17% window to wall ratio. This value for 40%,70% and 85% is 15–17%, while for 30% and 100% algae density, WWR is between 12-18% and 15–16%, sequentially.
5. In general, it can be concluded that using algae window in the cold BSk climate to achieve maximum daylighting and minimum energy consumption can be realized by integrating the low and medium algae densities of 20–40% and the low window-to-wall ratio of 10–25% in the north, south, and east. Only in the west, this technology can use any algae medium density to reach the optimization objectives, as long as window-to-wall ratio is within 12–18% window size range.

Table 8 lists the improvement percentages in EUI and UDI achieved by balanced design options as well as the average of all balanced options at four main orientations. By comparing the objective results of the best optimum solutions and objective results of the average value, it is observed that the optimization process results in an improvement in daylighting and energy saving. The average EUI improvement percentages across all optimum solutions are 39.67% and happen in the west (Tables 7 and 8). Besides, the north represents the lowest improvement in average EUI (i.e., 21.37%). The east and south stand at the second and the third in terms of energy-saving improvement when the design is optimized, respectively. In terms of improvement in optimized daylighting design, lesser overall improvement is seen in UDI, as compared with EUI, for all orientations. The improvement in UDI for north, south, east, and west include 4.60%, 14.43%, 13.34%, and 14.33%, respectively. According to Tables 7 and 8, the lowest total average UDI value for all densities occurs in the south, and the highest improvement after optimization happens in the south, too. Moreover, the north with the highest total average UDI value represents the lowest increase in percentile UDI improvement, after optimization.

### 3.4. Sensitivity analysis

Sensitivity analysis is a valid tool to investigate the complicated relationships between design variables and performance metrics [106–108]. It also helps to understand the most influential variables. By adjusting the input values, it can also help decrease uncertainties in the model outputs to small thresholds [109,110]. In this research, sensitivity analysis is applied to explore the relative contribution of design parameters to building performance indices including EUI and UDI.

In this research, the regression technique is used for sensitivity analysis, as a common method in building energy performance studies [111–114]. Besides, the multiple linear regression (MLR) using Standardized Regression Coefficients (SRC) was applied as a sensitivity

**Table 6**
Comparing energy simulation results with Negev et al. [29].

| | Algae Species | Algae-Win Concentration | | | | | | | | Climate | Orientation | | | | WWR | | | | | | Maximum energy Use differences compared with the base cases (kWh/m2/y) (Energy Savings) | | | Minimum energy Use differences compared with the base cases (kWh/m2/y) (None-savings) | | | Energy use differences in different façade orientations comparing with the base cases | | | Order of facades orientations in terms of energy saving |
|---|---|---|---|---|---|---|---|---|---|---|---|---|---|---|---|---|---|---|---|---|---|---|---|---|---|---|---|---|
| | | 20 | 30 | 40 | 50 | 60 | 70 | 85 | 100 | | N | S | E | W | 15 | 30 | 45 | 60 | 75 | 90 | Water-Win | DG-Win | SG-Win | Water-Win | DG-Win | SG-Win | SG-Win | DG- Win | Water-Win | |
| [29] | Chlorella vulgaris | | | | | | | | | Csa | | | | | | | | | | | South D:60% W:90% | South D:60% W:90% | South D:60% W:90% | North D:100% W:90% | North D:100% W:90% | North D:100% W:90% | North (+)[a] | North (+) | North (+) | 1 – South (Max.) SG-Win = 53.9% DG-Win = 29.6% Water-Win[c] |
| | | | | | | | | | | | | | | | | | | | | | | | | | | | South (+), (−)[b] | South (+), (−) | South (+), (−) | 2 – West SG-Win = 22.5% DG-Win = 16.1% Water-Win[c] |
| | | | | | | | | | | | | | | | | | | | | | | | | | | | East (+), (−) | East (+), (−) | East (+), (−) | 3 – East SG-Win = 13.8% DG-Win = 8.6% Water-Win[c] |
| | | | | | | | | | | | | | | | | | | | | | | | | | | | West (+), (−) | West (+), (−) | West (+), (−) | 4- North (+) SG-Win = 32.5% DG-Win = 36.1% Water-Win[c] |
| The Present Study | Chlorella vulgaris | | | | | | | | | BSk | | | | | | | | | | | West D:90% W:100% | West D:90% W:100% | West D:90% W:100% | North D:100% W:90% | North D:100% W:90% | North D:75% W:100% | North (+), (−) | North (+) | North (+) | 1 – South (Max.) SG-Win = 53.74% DG-Win = 47.11% Water-Win = 45.95% |
| | | | | | | | | | | | | | | | | | | | | | | | | | | | South (+), (−) | South (+), (−) | South (+), (−) | 2 – West SG-Win = 51.62% DG-Win = 41.91 Water-Win = 44.52% |
| | | | | | | | | | | | | | | | | | | | | | | | | | | | East (−) | East (+), (−) | East (−) | 3 – East SG-Win = 49.24% DG-Win = 40.52% Water-Win = 41.50% |
| | | | | | | | | | | | | | | | | | | | | | | | | | | | West (−) | West (+), (−) | West (−) | 4- North SG-Win = 10.18% DG-Win = 52.65% (+) Water-Win = 21.45% (+) |

D = Density, W=WWR.
[a] (+) = Non saving.
[b] (−) = Saving.
[c] Only energy Use differences (kWh/m2/y) was presented in Negev et al. [29].

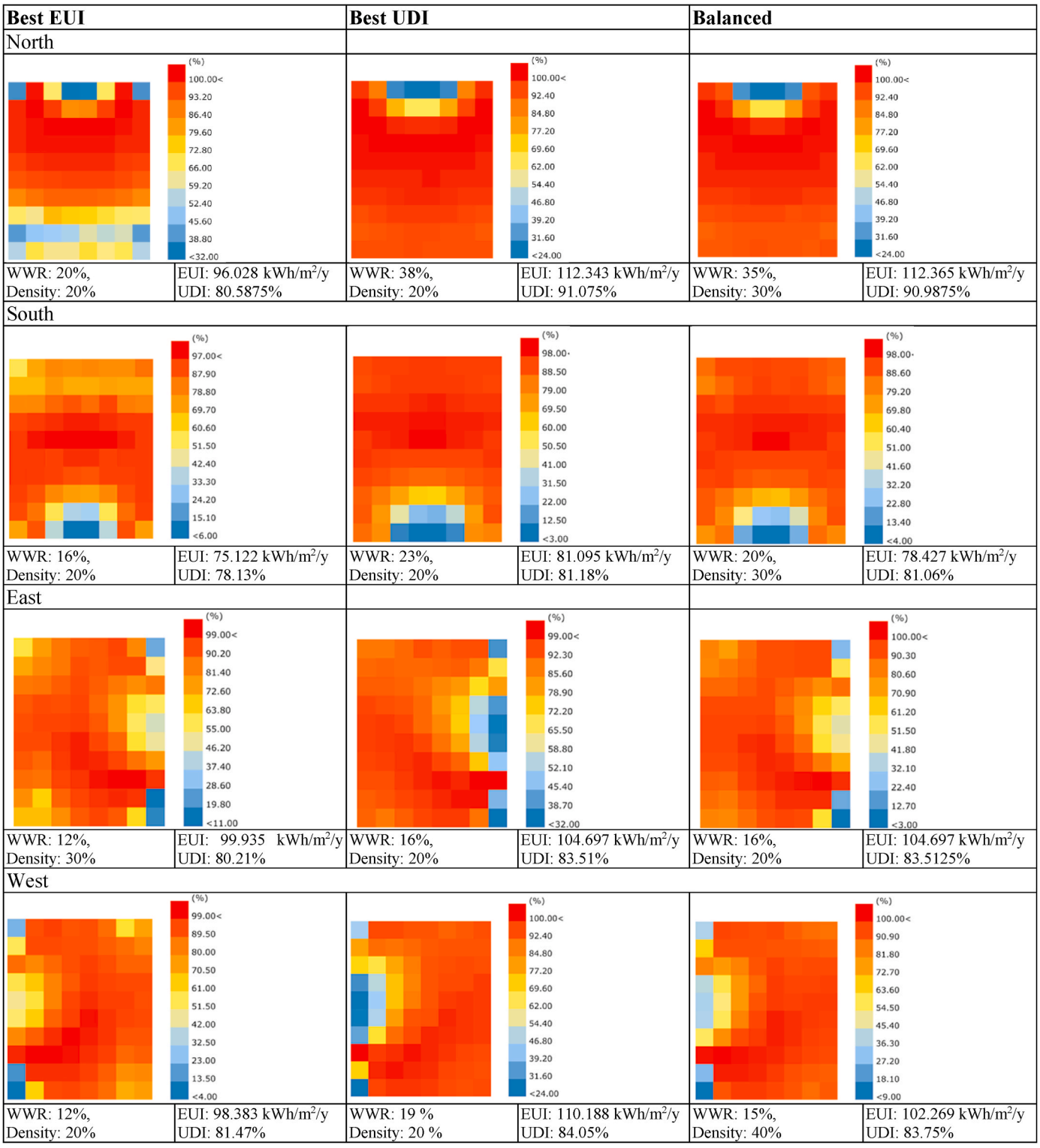


**Fig. 10.** Optimal design solutions including design options with the best EUI, the best UDI, and a selected balanced option.

analysis indicator, to investigate relative contributions of the design variables including window and algae medium density to building performance metrics (EUI and UDI) in the four main orientations. While Standardized Regression Coefficient is a normalized unit-less coefficient, Unstandardized Regression Coefficient (USRC) has units and a 'real-life' scale. High SRC absolute values would demonstrate a greater relative effect of one variable on performance indices. In other words, the higher the SRC value, the more impactful the independent parameter. Moreover, positive and negative SRC show positive and negative effects on performance metrics, respectively. In this study, all the 2560 design options, and not just the optimized solutions, were used for sensitivity analysis.

Table 10 indicates the USRC and SRC values of two design variables including window-to-wall (WWR) ratio and algae concentration, for daylighting and energy use intensity. The corresponding values are determined by considering all building orientations. The higher values

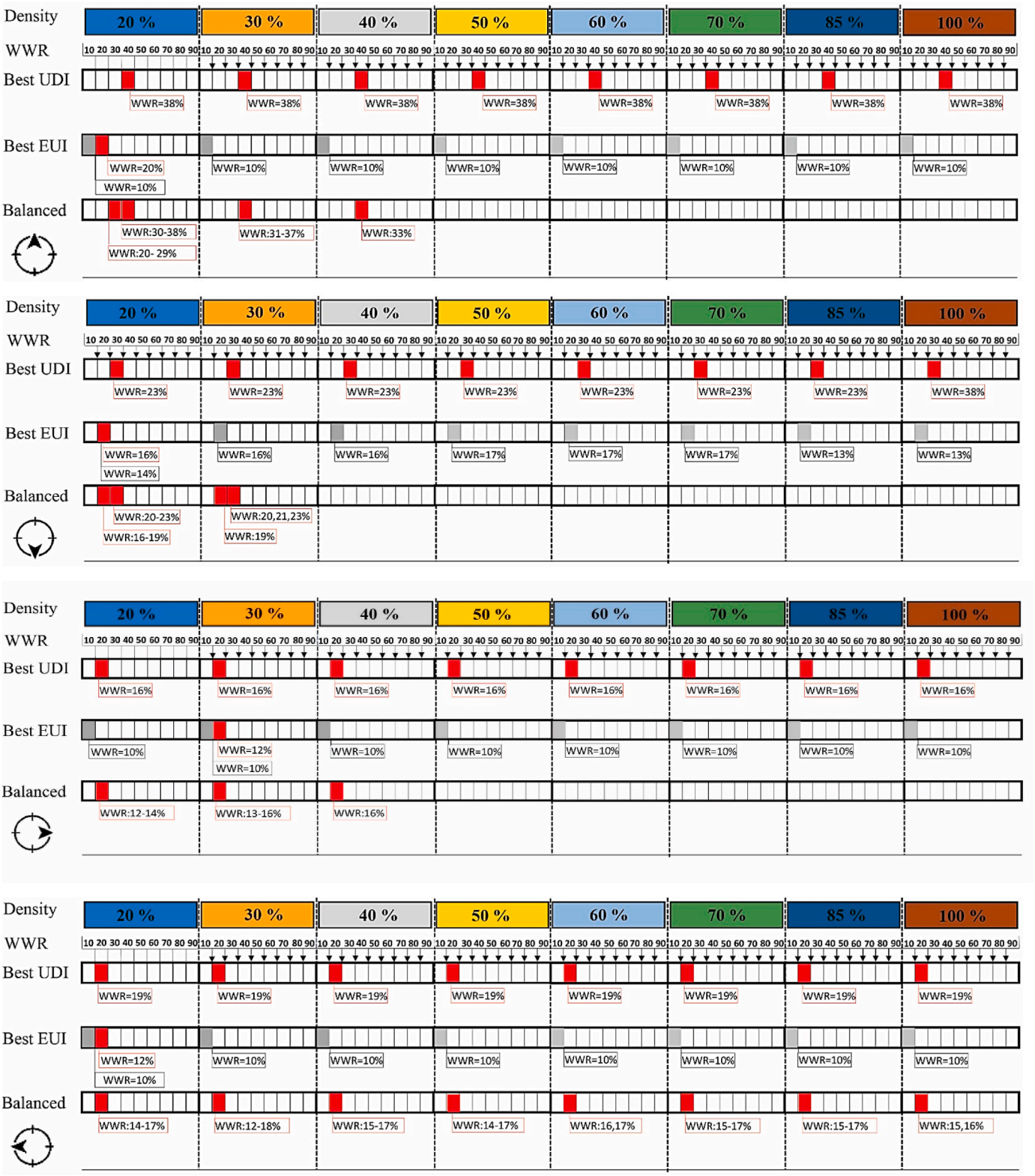


**Fig. 11.** The optimum design solutions in terms of Best EUI, UDI, and the balanced options at each orientation.

indicate that the variable of interest has a higher impact on both performance metrics. In terms of EUI, the USRC values of algae density and WWR for north, south, east, and west are 23.275, 114.786; −9.496, 119.052; −31.514, 173.572, and −49.951, 206.021, respectively and sequentially. By comparing the regression coefficients, it is observed that WWR in all orientations in the BSk climate has a greater effect on both energy and daylighting performance. Contrary to WWR, algae density's impact on UDI is ignorable in all orientations. Fig. 12 illustrates the effects. Sensitivity analysis results also show that, except for the north, algae density in all other orientations is negatively correlated with energy use intensity. Also, both algae concentration and WWR have the strongest effects on EUI in the north. East orientation takes the

**Table 7**
Minimum and Maximum EUI and UDI values and their averages for façade orientations.

| Orientation | Maximum and Minimum EUI and UDI based on each algae density and WWR | | | | | | | | | | | | Total Average for all densities | | | | | | | | | |
|---|---|---|---|---|---|---|---|---|---|---|---|---|---|---|---|---|---|---|---|---|---|---|
| | Max EUI (kWh/m$^2$/y) | | | Min EUI (kWh/m$^2$/y) | | | Min UDI (%) | | | Max UDI (%) | | | | | Average EUI based on different algae density | | | | | | | |
| | WWR | Density | Value | WWR | Density | Value | WWR | Density | Value | WWR | Density | Value | UDI | EUI | 20% | 30% | 40% | 50% | 60% | 70% | 85% | 100% |
| North | 90% | 100% | 197.02 | 10% | 20% | 88.04 | 10% | 20–100 | 50.23 | 38% | 20–100 | 91.07 | 85.27 | 135.85 | 124.55 | 127.66 | 133.95 | 136.52 | 138.68 | 140.26 | 141.84 | 143.31 |
| South | 90% | 20% | 215.63 | 14% | 20% | 74.67 | 90% | 20–100 | 56.5 | 23% | 20–100 | 81.18 | 70.33 | 117.20 | 131.78 | 121.21 | 112.93 | 111.41 | 111.22 | 112.30 | 116.08 | 120.67 |
| East | 90% | 20% | 289.76 | 10% | 20% | 97.4 | 90% | 20–100 | 58.92 | 16% | 20–100 | 83.51 | 72.62 | 160.36 | 185.79 | 171.45 | 158.18 | 154.15 | 152.02 | 151.15 | 153.47 | 156.72 |
| West | 90% | 20% | 334.74 | 10% | 20% | 95.35 | 90% | 20–100 | 58.62 | 19% | 20–100 | 84.05 | 73.16 | 171.22 | 205.00 | 187.69 | 171.47 | 165.63 | 162.13 | 160.38 | 159.00 | 158.44 |

**Table 8**
Improvement percentage of some selected balanced optimal solutions as well as the average improvement percentage of all balanced options.

| | Improvement percentage of some balanced options | | | | | | | | | | | | | | | | | | | | | | | | Average improvement percentage of all balanced options | |
|---|---|---|---|---|---|---|---|---|---|---|---|---|---|---|---|---|---|---|---|---|---|---|---|---|---|---|
| | Size | UDI | EUI | Size | UDI | EUI | Size | UDI | EUI | Size | UDI | EUI | Size | UDI | EUI | Size | UDI | EUI | Size | UDI | EUI | Size | UDI | EUI | UDI | EUI |
| North | W-30% D-20% | 5.55% | 21.98% | W-38% D-20% | 6.80% | 17.30% | W-20% D-20% | 5.50% | 29.31% | W-29% D-20% | 5.39% | 22.56% | W-31% D-30% | 6.02% | 19.75% | W-35% D-30% | 6.69% | 17.29% | W-37% D-30% | 6.63% | 15.89% | W-33% D-40% | 6.39% | 15.39% | 4.60% | 21.37% |
| South | W-16% D-20% | 11.09% | 35.90% | W-19% D-20% | 14.40% | 33.96% | W-20% D-20% | 15.25% | 34.07% | W-23% D-20% | 15.42% | 30.81% | W-19% D-30% | 14.40% | 32.93% | W-20% D-30% | 15.25% | 33.08% | W-21% D-30% | 15.28% | 31.91% | W-23% D-30% | 15.42% | 30.95 | 14.43% | 33.25% |
| East | W-12% D-20% | 9.46% | 37.64% | W-13% D-20% | 12.32% | 36.66% | W-14% D-20% | 13.74% | 35.89% | W-13% D-30% | 12.32% | 36.79% | W-14% D-30% | 13.74% | 36.29% | W-15% D-30% | 14.23% | 35.65% | W-16% D-30% | 14.99% | 35.35% | W-16% D-40% | 14.99% | 35.47% | 13.34% | 36.22% |
| West | W-14% D-20% | 14.16% | 41.98% | W-12% D-30% | 11.35% | 42.30% | W-16% D-40% | 14.57% | 40.28% | W-15% D-50% | 14.47% | 39.93% | W-17% D-60% | 14.63% | 38.71% | W-16% D-70% | 14.57% | 39.50% | W-17% D-85% | 14.63% | 37.72% | W-17% D-100% | 14.63% | 37.52% | 14.33% | 39.67% |

**Table 9**
Result comparison between the first and the second optimization method in terms of design parameters.

| | North | South | East | West |
|---|---|---|---|---|
| First method | D: 20%<br>W: 20–29%, 30–38%<br>D:30%<br>W: 31–37%<br>D:40%<br>W: 33% | D: 20%<br>W: 16–23%<br>D: 30%<br>W: 19–21%, 23% | D: 20%<br>W: 12–14%<br>D: 30%<br>W: 13–16%<br>D: 40%<br>W: 16% | D: 20%, 50%<br>W:14–17%<br>D:30%<br>W:12–18%<br>D: 40%,70%,85%<br>W:15–17%<br>D:60%<br>W:16–17%<br>D:100%<br>W:15–16% |
| Second method | D: 20%<br>W: 25–28%<br>D:30%<br>W: 35% | D: 20%<br>W: 15–21%<br>D:30%<br>W: 17–20%<br>D:40%<br>W: 12% | D: 30%<br>W: 13–15%<br>D: 40%<br>W: 16%<br>D: 50%<br>W: 16% | D: 20%<br>W:15%<br>D:30%<br>W:14–18%<br>D: 40%,70%<br>W: 17%<br>D:50%<br>W: 13–17%<br>D:60%<br>W:17–18% |

D = Density W=WWR.

second rank in the effect of WWR on EUI, followed by south and west. In terms of algae density, east stands second, followed by west and south. WWR also has a negative correlation with UDI in the south, east, and west, and a positive correlation with it in the north.

## 4. Validation

### 4.1. Validation of building performance simulator

In this research, to evaluate the accuracy of the results, the Honeybee plugin applying OpenStudio and EnergyPlus engines for energy simulation was validated to examine the precision of its data and consequent results using the comparison method. Honeybee plugin an old version of 0.0.64 was validated in a previous study [115]. In the present study, the results of the Honeybee plugin version of 0.0.69 were compared with the validated sample. Besides, this paper added the validation of the annual solar radiation results (Fig. 14 and A1-A2 in appendix), not embedded in [115], to the evaluation process, along with evaluating annual heating and cooling energy. Validation has been conducted by case No.600 (BESTest) in the ASHRAE Standard 140–2017 [62]. Case No.600 is categorized as Class I Test Procedures, analyzing the ability of software to model building in a low-mass configuration (Fig. 13). There are the low mass basic tests applying lightweight walls, floor, and roof, whose details are described in the standard [62]. Consequently, by comparing the results of the Honeybee simulation with the BESTest (Figss. 14–18, Figs. A1 and A2) it can be inferred that Honeybee could get the sample 600 (BESTest) validation showing the accuracy of the simulation results. In general, the result of the simulation is in accordance with ASHRAE 140–2017 standard validation [62].

## 5. Conclusion

This research bridges the knowledge gaps in adopting microalgae photobioreactors as window systems in the building by achieving two main objectives including to study the effects of building-integrated microalgae windows on energy savings in the BSk climate and to

**Table 10**
SRC and USRC of design variables.

| Group | Variable | EUI | | | | UDI | | | |
|---|---|---|---|---|---|---|---|---|---|
| | | Unstandardized Coefficients | | Standardized Coefficients | R Square | Unstandardized Coefficients | | Standardized Coefficients | R Square |
| | | B | Std. Error | Beta | | B | Std. Error | Beta | |
| North | (Constant) | 65.222 | .466 | | .983 | 76.233 | 1.049 | | .209 |
| | Density | 23.275 | .561 | .215 | | .000 | 1.263 | .000 | |
| | WWR | 114.786 | .615 | .968 | | 18.078 | 1.384 | .457 | |
| South | (Constant) | 63.080 | 1.346 | | .875 | 84.818 | .421 | | .808 |
| | Density | −9.496 | 1.622 | -.081 | | .000 | .508 | .000 | |
| | WWR | 119.052 | 1.777 | .932 | | −28.957 | .556 | -.899 | |
| East | (Constant) | 91.505 | 1.513 | | .924 | 88.749 | .230 | | .946 |
| | Density | −31.514 | 1.823 | -.188 | | .000 | .277 | .000 | |
| | WWR | 173.572 | 1.996 | .943 | | −32.256 | .304 | -.973 | |
| West | (Constant) | 94.802 | 6.246 | | .509 | 90.089 | .237 | | .948 |
| | Density | −49.951 | 7.525 | -.183 | | .000 | .285 | .000 | |
| | WWR | 206.021 | 8.242 | .690 | | −33.853 | .313 | -.974 | |

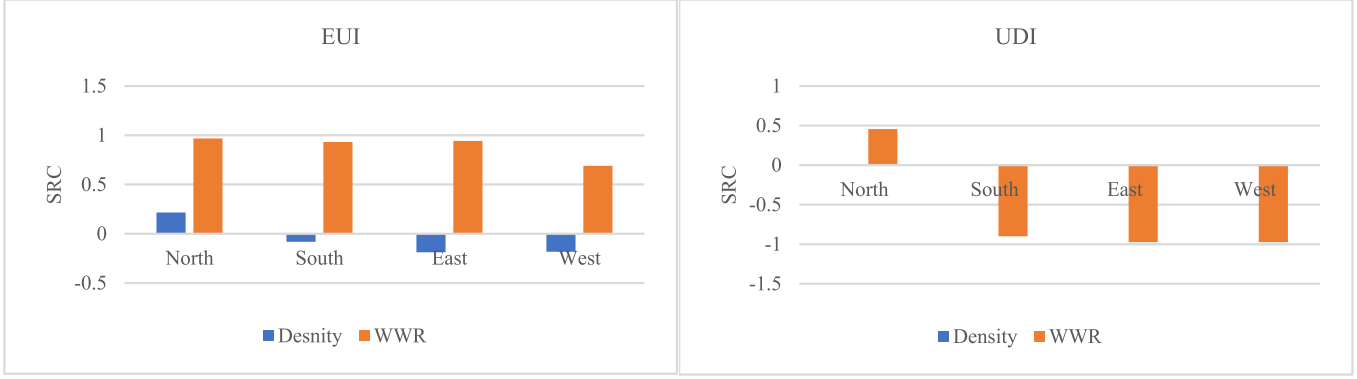


**Fig. 12.** SRC for design variables including algae density and window size on EUI and UDI.

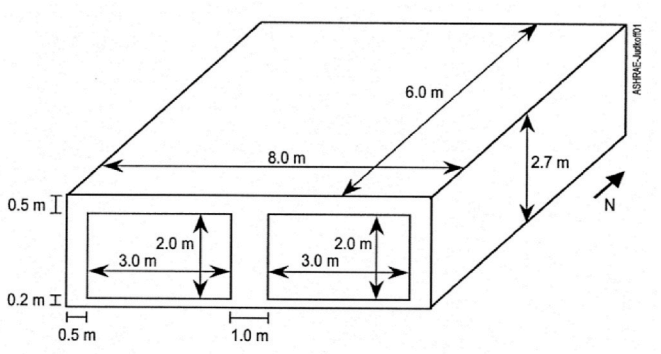


**Fig. 13.** Sample testing Case. Case No.600. ASHRAE Standard 140–2017 [62].

develop an optimization framework to identify algae PBR design solutions that lead to best energy and daylighting performance in buildings. To achieve the first goal, the energy efficiency of building-integrated PBR was compared with that of three reference cases with single-glazed, double-glazed, and water windows, in four main orientations (Tables A1-A3). The results show that the PBR window has the potential to greatly improve building energy efficiency in the BSk climate. The multi-objective framework can evaluate the daylighting and energy function of the building-integrated PBRs as a green building façade while proposing the optimal design solutions for each orientation. The variables of interest in this research included microalgae density and window-to-wall ratio in four building orientations. Sample testing case No.600 (BESTest) (Fig. 13), was applied to validate the simulation software results. According to Fig. 14–18 and Fig. A1-A2 comparing the simulation results with the BESTest, the Honeybee plugin could get a sample 600 (BESTest) validation. The results of this research also reveal several design strategies for integrating algae windows into building façade and achieving optimum energy and daylighting performance, as follows:

(a) The energy performance of the building-integrated microalgae PBR is affected by façade orientation. The south orientation surpasses the other three orientations in terms of energy performance improvement, followed by the west and east. In the north, using algae window leads to no improvement in energy efficiency, as compared with the reference cases, except when algae density is low in comparison to SG-Win. The results demonstrate that given algae densities and WWRs in the south, east, and west can have considerable effects on energy consumption. As a general rule of thumb, the higher WWR and denser algae medium result in greater energy efficiency in algae windows compared to the three reference cases. In the north and with low algae densities, there are some exceptions to this rule. Considering all three reference cases and all orientations, the maximum energy use differences occur in the highest window to wall ratios (i.e., 90% in this research). The algae density of 70% in the south and east and algae density of 100% in the west lead to the highest energy savings. In the north and only in comparison with the SG-Win, there was a 10.18% decrease in energy consumption where the WWR and density were 100% and 20%, respectively (Table 5).

(b) The effectiveness of the proposed multi-objective optimization framework was shown by its ability to identify design combinations with optimum energy savings and daylight improvements for building-integrated PBRs. This method was evaluated by applying an evolutionary algorithm using the Octopus Grasshopper plugin which is based on Genetic Algorithm (SPEA-2 multi-objective algorithm) and Hypervolume Estimation

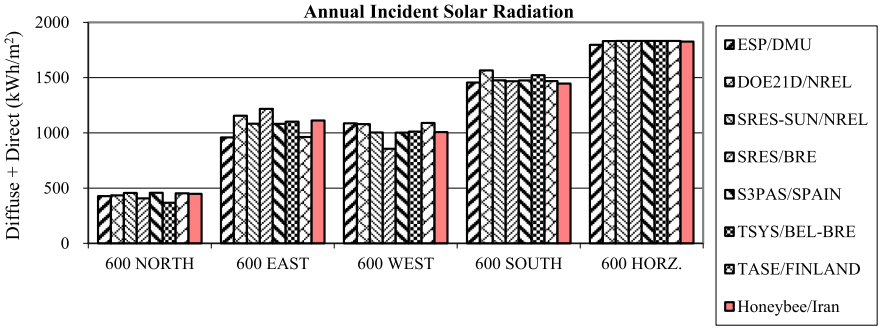


**Fig. 14.** Comparison of the results derived from Annual Incident Solar Radiation.
Program: ESP-RV8, Implemented by: De Montfort University, U.K.
Program: BLAST-3.0 Level 193 v.1, Implemented by NREL1, U.S. Politecnico Torino, Italy.
Program: DOE-2.1D 14, Implemented by NREL, U.S.
Program: SERIRES/SUNCODE
5.7, Implemented by NREL, U.S.
Program: SERIRES 1.2, Implemented by BRE2, U.K.
Program: S3PAS, Implemented by University of Sevilla, Spain.
Program: TRNSYS 13.1, Implemented by BRE, U.K.; Vrije Universiteit, Belgium.
Program: TASE, Implemented by Tampere University, Finland.

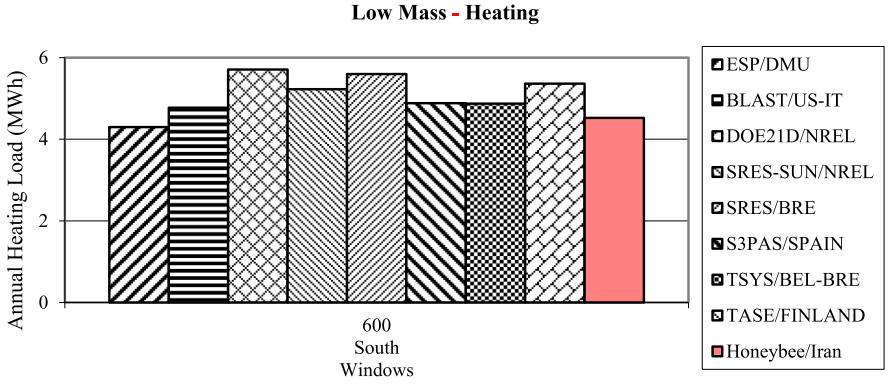


**Fig. 15.** Comparison of the results derived from low mass annual heating energy.

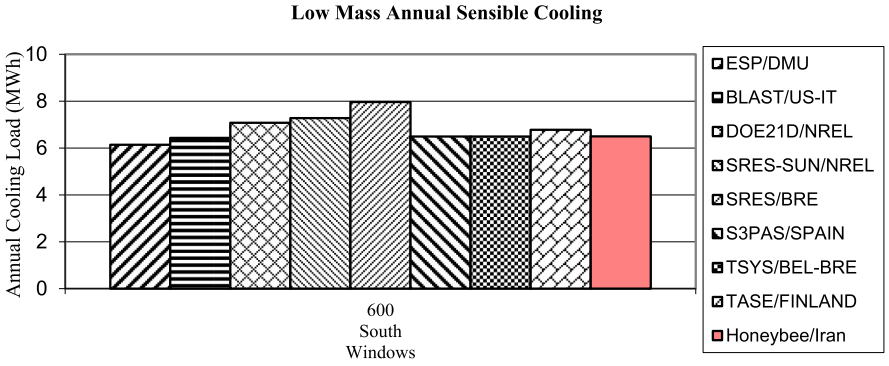


**Fig. 16.** Comparison of the results derived from low mass annual cooling energy.

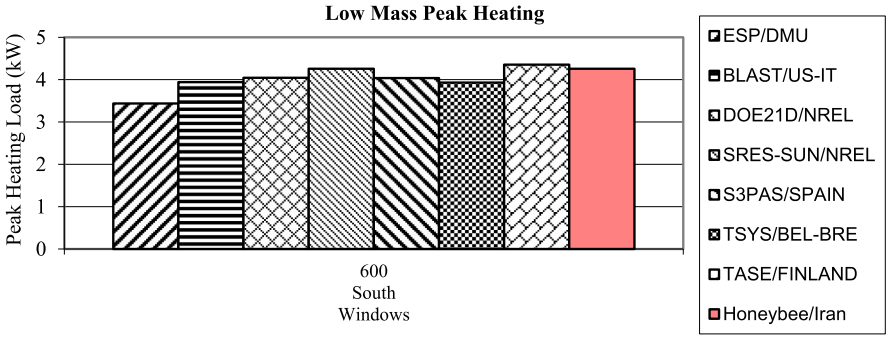


**Fig. 17.** Comparison of the results derived from peak heating load.

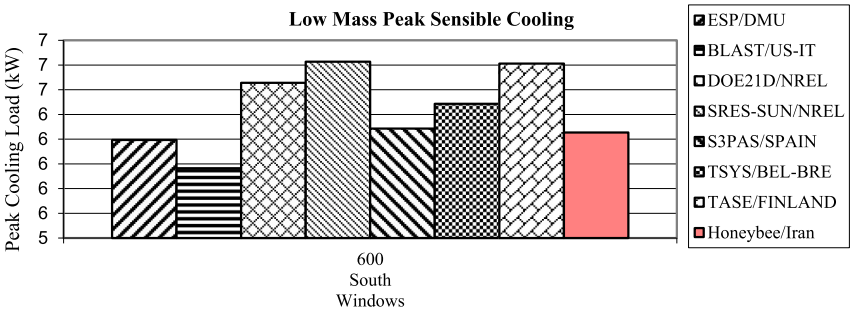


**Fig. 18.** Comparison of the results derived from peak cooling load.

Algorithm (HypE). The optimization framework increased the simulation-based average EUI values by 21.37%, 33.25%, 36.22%, 39.67%, and the average UDI values by 4.60%, 14.43%, 13.34%, and 14.33% in the north, south, east, and west, respectively. The optimized design options in the north, south, and east would have low algae densities as well as a low window-to-wall ratio, while the optimum results for the west would include any algae density and low window-to-wall ratio. When in an office building in the BSk climate, saving in energy is the only objective, the greater WWR, and denser algae medium lead to better performance improvements. However, when daylighting performance is integrated with energy efficiency, the optimum solutions are limited to the low WWR and low algae density, except for the west as mentioned above. The results of multi-objective optimization conducted by the second method using Octopus also certifies the results achieved by the first method. In general, Table 9 shows that according to the two methods the optimum design options include low WWR for all building orientations and low algae density for all building aspects except for the West which includes all studied algae concentrations according to the first method. However, the number of Pareto solutions suggested by Octopus is more limited than that of Pareto suggested by the first method although they fall within the same range. Hence, best solutions were suggested based on the wider range of results in method 1 for designers

(c) The regression analysis showed that two design variables (window size, and algae density) in four main building orientations differently impact the two studied performance metrics (EUI and UDI). WWR yields the largest effects on energy consumption in all orientations, while its large impact is negatively related to UDI metrics in all orientations, except north. Also, without considerable effect on UDI, algae density negatively affects energy performance in all orientations, except for the north. The results show that applying algae window with high WWR is beneficial in

the north only when UDI is considered. However, the positive effect of algae density and WWR on EUI in this orientation shows that in general, the higher window size and algae density, the higher energy consumption. In the south, east, and west the higher WWR also results in higher energy consumption, while with more algae density there is more energy efficiency in a general trend.

Overall, In the BSk climate, larger WWR results in higher energy consumption across all studied cases (single-glazed, double-glazed, water, and algae windows). Besides, optimization results demonstrate that algae window with high WWR and high density acts imperfectly in providing low energy consumption as well as high UDI. The favorable orientations for applying algae windows in the BSk climate are south and west. Finally, further research needs to study the effects of algae window design on other performance metrics such as thermal and visual comfort, cost, and life cycle impacts. The potential of adaptable shading of the algae window can be investigated based on the proposed performance metrics, too. Also, the proposed framework must be complemented by adding more design variables and exploring their effects on other building types and climate zones.

## Funding

This research did not receive any specific grant from funding agencies in the public, commercial, or not-for-profit sectors.

## Declaration of competing interest

The authors declare that they have no known competing financial interests or personal relationships that could have appeared to influence the work reported in this paper.

## Appendix

**Table A1**
Annual energy consumption between PBR window and SG-Win.

| Orientation | Window Size (%) | Energy use differences in kWh/m$^2$/y according to microalgae concentration and Window size | | | | | | | |
|---|---|---|---|---|---|---|---|---|---|
| | | Density (%) | | | | | | | |
| | | 100 | 85 | 70 | 60 | 50 | 40 | 30 | 20 |
| North | 15 | 4.340948 | 3.932885 | 3.932885 | 3.005125 | 2.386942 | 1.672491 | −0.797933 | −2.567626 |
| | 30 | 11.802134 | 11.019629 | 10.217555 | 9.339973 | 8.176887 | 6.771918 | 2.817305 | 0.456529 |
| | 45 | 12.670939 | 11.375206 | 10.059088 | 8.697341 | 6.827619 | 4.536559 | −1.053469 | −4.094638 |
| | 60 | 13.515775 | 11.672321 | 9.777274 | 7.856825 | 5.205026 | 2.017871 | −5.462457 | −8.975554 |
| | 75 | 13.944976 | 11.554351 | 9.133868 | 6.702171 | 3.34515 | −0.652262 | −9.8127 | −14.02531 |
| | 90 | 13.798488 | 10.897347 | 7.965045 | 5.040547 | 1.004732 | −3.789922 | −14.521275 | −18.666329 |
| South | 15 | 4.99971 | 4.5721 | 4.61023 | 4.93149 | 5.81436 | 3.9181 | −1.479372 | −3.877817 |
| | 30 | −24.58536 | −26.7075 | −28.66701 | −30.74377 | −33.06924 | −34.73389 | −35.48865 | −32.96746 |
| | 45 | −58.24399 | −66.55217 | −69.85764 | −72.3286 | −73.21487 | −73.03984 | −67.22701 | −58.24399 |
| | 60 | −97.79849 | −103.3889 | −108.1175 | −109.9386 | −109.5884 | −107.2728 | −94.56369 | −80.42417 |
| | 75 | −130.9703 | −138.7537 | −144.8699 | −145.5105 | −143.8355 | −139.1632 | −120.3463 | −100.3378 |
| | 90 | −162.7851 | −171.6569 | −179.0851 | −178.2813 | −175.2973 | −168.2941 | −143.7579 | −117.6072 |
| East | 15 | −9.54186 | −9.82934 | −10.166842 | −10.673384 | −11.058619 | −11.215579 | −12.322466 | −11.769462 |
| | 30 | −49.781112 | −52.287389 | −53.549881 | −53.551273 | −53.170563 | −52.172681 | −47.790558 | −40.882918 |
| | 45 | −89.299224 | −91.693226 | −94.352962 | −94.080631 | −92.508665 | −89.348429 | −78.121554 | −65.45805 |
| | 60 | −127.463943 | −131.289464 | −134.703478 | −133.304654 | −130.371974 | −125.077036 | −107.549596 | −89.390206 |
| | 75 | −163.424765 | −168.410868 | −171.90347 | −169.76765 | −165.476004 | −157.822216 | −134.301991 | −110.551603 |
| | 90 | −196.441997 | −202.626233 | −205.995608 | −203.190224 | −197.374507 | −187.634872 | −157.945209 | −128.515124 |
| West | 15 | −12.562877 | −13.504593 | −14.424922 | −14.523174 | −15.249388 | −15.820285 | −17.005732 | −15.986124 |
| | 30 | −58.612391 | −59.964094 | −60.010121 | −59.98044 | −59.276611 | −57.573311 | −51.534835 | −43.24756 |
| | 45 | −110.102157 | −110.215712 | −109.198551 | −107.89194 | −105.180998 | −100.453853 | −86.470049 | −71.151811 |
| | 60 | 158.823663 | 157.224676 | 155.220718 | 152.771592 | 147.969221 | 140.247278 | 118.844628 | −96.783331 |
| | 75 | −202.880613 | −200.558108 | −197.448328 | −193.624026 | −186.749983 | −176.049999 | −147.349287 | −118.512685 |
| | 90 | −243.558746 | −240.394583 | −236.218735 | −231.201714 | −222.211618 | −208.525669 | −172.416559 | −137.021615 |

**Table A2**
Annual energy consumption between PBR window and DG-Win.

| Orientation | Window Size (%) | Energy use differences in kWh/m$^2$/y according to microalgae concentration and Window size | | | | | | | |
|---|---|---|---|---|---|---|---|---|---|
| | | Density (%) | | | | | | | |
| | | 100 | 85 | 70 | 60 | 50 | 40 | 30 | 20 |
| North | 15 | 10.749247 | 10.341184 | 9.922543 | 9.413424 | 8.795241 | 8.08079 | 5.610366 | 3.840673 |
| | 30 | 27.585252 | 26.802748 | 26.000673 | 25.123091 | 23.960005 | 22.555037 | 18.600423 | 16.239648 |
| | 45 | 38.248969 | 36.953237 | 35.637118 | 34.275371 | 32.40565 | 30.11459 | 24.524561 | 21.483392 |
| | 60 | 49.091105 | 47.247651 | 45.352604 | 43.432155 | 40.780356 | 37.593202 | 30.112873 | 26.599776 |
| | 75 | 59.115526 | 56.7249 | 54.304418 | 51.872721 | 48.5157 | 44.518287 | 35.35785 | 31.14524 |
| | 90 | 67.961499 | 65.060358 | 62.128056 | 59.203558 | 55.167743 | 50.373089 | 39.641736 | 35.496682 |
| South | 15 | 12.670266 | 12.242657 | 12.280787 | 12.602047 | 13.48492 | 11.588658 | 6.191184 | 3.792738 |
| | 30 | −6.741672 | −8.863805 | −10.823325 | −12.900085 | −15.225547 | −16.890196 | −17.644964 | −15.123769 |
| | 45 | −37.849243 | −42.032118 | −45.337589 | −47.808555 | −48.694818 | −48.519791 | −42.706958 | −33.723944 |
| | 60 | −66.794208 | −72.384653 | −77.113253 | −78.934359 | −78.584163 | −76.268544 | −63.559415 | −49.41989 |
| | 75 | −94.16805 | −101.951477 | −108.067638 | −108.708282 | −107.033273 | −102.360933 | −83.544078 | −63.53557 |

(*continued on next page*)

**Table A2** (*continued*)

| Orientation | Window Size (%) | Energy use differences in kWh/m$^2$/y according to microalgae concentration and Window size | | | | | | | |
|---|---|---|---|---|---|---|---|---|---|
| | | Density (%) | | | | | | | |
| | | 100 | 85 | 70 | 60 | 50 | 40 | 30 | 20 |
| | 90 | −121.032858 | −129.90463 | −137.332844 | −136.529048 | −133.545038 | −126.541811 | −102.005667 | −75.854924 |
| East | 15 | 2.408574 | 2.121093 | 1.783591 | 1.277049 | 0.891814 | 0.734855 | −0.372032 | 0.180972 |
| | 30 | −24.406442 | −26.912719 | −28.175211 | −28.176604 | −27.795893 | −26.798011 | −22.415888 | −15.508248 |
| | 45 | −52.05399 | −54.447991 | −57.107728 | −56.835396 | −55.26343 | −52.103195 | −40.876319 | −28.212816 |
| | 60 | −80.768304 | −84.593825 | −88.007839 | −86.609014 | −83.676334 | −78.381396 | −60.853956 | −42.694566 |
| | 75 | −108.682256 | −113.668359 | −117.160961 | −115.02514 | −110.733495 | −103.079707 | −79.559482 | −55.809094 |
| | 90 | −135.086862 | −141.271099 | −144.640474 | −141.835089 | −136.019372 | −126.279737 | −96.590074 | −67.159989 |
| West | 15 | 1.940909 | 0.999192 | 0.078864 | −0.019388 | −0.745603 | −1.316499 | −2.501946 | −1.482338 |
| | 30 | −27.535208 | −28.886912 | −28.932938 | −28.903258 | −28.199429 | −26.496129 | −20.457652 | −12.170378 |
| | 45 | −64.036654 | −64.150208 | −63.133047 | −61.826436 | −59.115494 | −54.388349 | −40.404545 | −25.086307 |
| | 60 | −99.834366 | −98.235379 | −96.231421 | −93.782295 | −88.979924 | −81.257982 | −59.855332 | −37.794034 |
| | 75 | −132.987416 | −130.664912 | −127.555132 | −123.73083 | −116.856786 | −106.156803 | −77.456091 | −48.619489 |
| | 90 | −164.656179 | −161.492016 | −157.316168 | −152.299147 | −143.309051 | −129.623102 | −93.513992 | −58.119048 |

**Table A3**
Annual energy consumption between PBR window and Water-Win.

| Orientation | Window Size (%) | Energy use differences in kWh/m$^2$/y according to microalgae concentration Window size | | | | | | | |
|---|---|---|---|---|---|---|---|---|---|
| | | Density (%) | | | | | | | |
| | | 100 | 85 | 70 | 60 | 50 | 40 | 30 | 20 |
| North | 15 | 11.057258 | 10.649195 | 10.230554 | 9.721434 | 9.103252 | 8.3888 | 5.918376 | 4.148684 |
| | 30 | 15.818762 | 15.036257 | 14.234183 | 13.356601 | 12.193515 | 10.788546 | 6.833933 | 4.473158 |
| | 45 | 21.121992 | 19.82626 | 18.510141 | 17.148395 | 15.278673 | 12.987613 | 7.397584 | 4.356415 |
| | 60 | 26.184663 | 24.341209 | 22.446161 | 20.525713 | 17.873914 | 14.686759 | 7.206431 | 3.693333 |
| | 75 | 30.830654 | 28.440028 | 26.019546 | 23.587849 | 20.230827 | 16.233415 | 7.072977 | 2.860368 |
| | 90 | 34.808256 | 31.907115 | 28.974813 | 26.050314 | 22.0145 | 17.219846 | 6.488493 | 2.343439 |
| South | 15 | 9.76365 | 9.33604 | 9.37417 | 9.695431 | 10.578303 | 8.682042 | 3.284567 | 0.886122 |
| | 30 | −8.029838 | −10.151971 | −12.11149 | −14.18825 | −16.513712 | −18.178362 | −18.933129 | −16.411935 |
| | 45 | −35.771095 | −39.95397 | −43.259441 | −45.730407 | −46.61667 | −46.441643 | −40.62881 | −31.645796 |
| | 60 | −62.602988 | −68.193432 | −72.922033 | −74.743139 | −74.392943 | −72.077324 | −59.368195 | −45.22867 |
| | 75 | −88.796454 | −96.579881 | −102.696042 | −103.336687 | −101.661678 | −96.989337 | −78.172482 | −58.163974 |
| | 90 | −114.797794 | −123.669567 | −131.09778 | −130.293985 | −127.309974 | −120.306748 | −95.770603 | −69.61986 |
| East | 15 | −1.451624 | −1.739105 | −2.076607 | −2.583149 | −2.968384 | −3.125343 | −4.23223 | −3.679226 |
| | 30 | −29.537331 | −32.043608 | −33.3061 | −33.307492 | −32.926782 | −31.9289 | −27.546777 | −20.639137 |
| | 45 | −57.543441 | −59.937443 | −62.597179 | −62.324848 | −60.752882 | −57.592646 | −46.365771 | −33.702267 |
| | 60 | −85.903465 | −89.728986 | −93.143 | −91.744175 | −88.811495 | −83.516557 | −65.989117 | −47.829728 |
| | 75 | −114.226544 | −119.212647 | −122.705249 | −120.569429 | −116.277783 | −108.623996 | −85.103771 | −61.353383 |
| | 90 | −141.081881 | −147.266118 | −150.635493 | −147.830108 | −142.014391 | −132.274756 | −102.585093 | −73.155008 |
| West | 15 | −3.323522 | −4.265239 | −5.185567 | −5.283819 | −6.010034 | −6.580931 | −7.766378 | −6.746769 |
| | 30 | −36.014599 | −37.366303 | −37.412329 | −37.382649 | −36.67882 | −34.975519 | −28.937043 | −20.649768 |
| | 45 | −75.149846 | −75.263401 | −74.24624 | −72.939629 | −70.228686 | −65.501542 | −51.517738 | −36.199499 |
| | 60 | −113.641749 | −112.042762 | −110.038804 | −107.589678 | −102.787307 | −95.065364 | −73.662714 | −51.601417 |
| | 75 | −149.276856 | −146.954352 | −143.844572 | −140.02027 | −133.146226 | −122.446242 | −93.745531 | −64.908929 |
| | 90 | −183.162803 | −179.998641 | −175.822792 | −170.805772 | −161.815675 | −148.129727 | −112.020616 | −76.625672 |

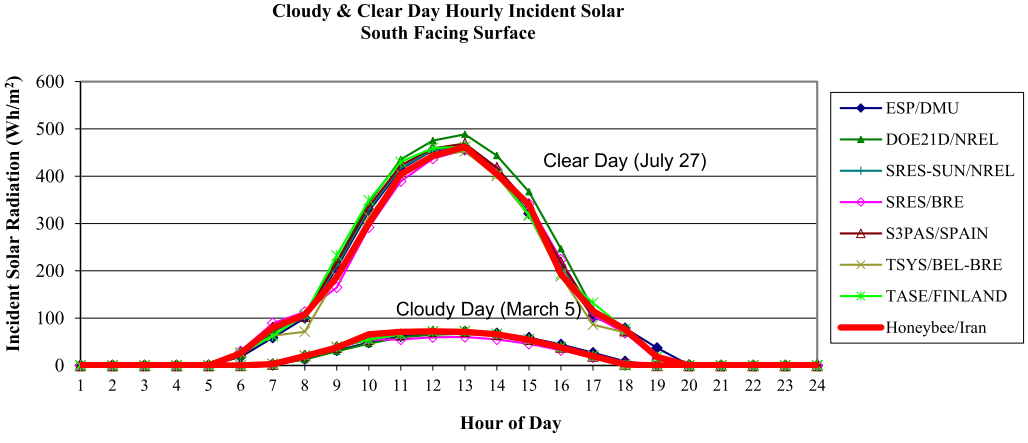


**Fig. A1.** Comparison the results derived from incident solar radiation (South surface)

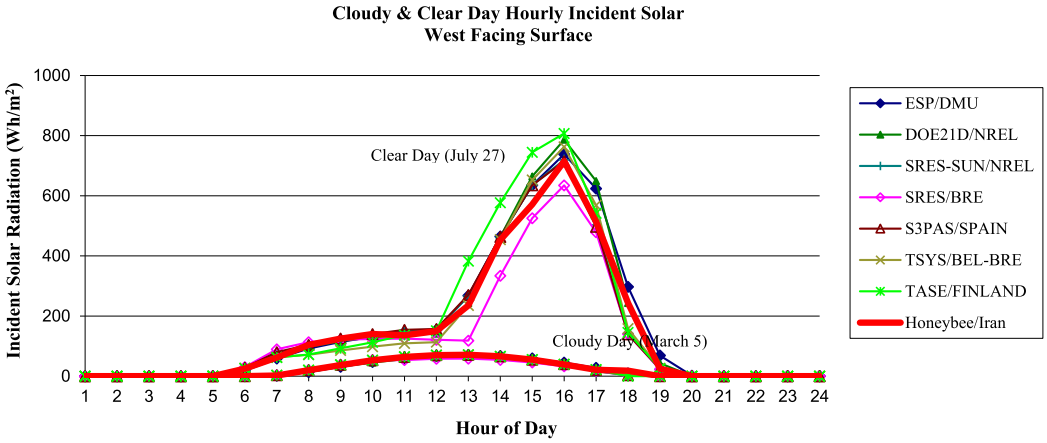


**Fig. A2.** Comparison the results derived from incident solar radiation (West surface)

## Appendix A. Supplementary data

Supplementary data to this article can be found online at https://doi.org/10.1016/j.jobe.2021.102832.

## References


[1] T. Wang Cai, S. Wang, L. Cozzi, B. Motherway, D. Turk, Towards a Zero-Emission, Efficient, and Resilient Buildings and Construction Sector, 2017.

[2] T. Zhang, H. Yang, Flow and heat transfer characteristics of natural convection in vertical air channels of double-skin solar façades, Appl. Energy 242 (2019) 107–120, https://doi.org/10.1016/j.apenergy.2019.03.072.

[3] I. Hernández-López, J. Xamán, I. Zavala-Guillén, I. Hernández-Pérez, P. Moreno-Bernal, Y. Chávez, Thermal performance of a solar façade system for building ventilation in the southeast of Mexico, Renew. Energy 145 (2020) 294–307, https://doi.org/10.1016/j.renene.2019.06.026.

[4] C.M. Lai, S. Hokoi, Solar façades: a review, Build. Environ. 91 (2015) 152–165, https://doi.org/10.1016/j.buildenv.2015.01.007.

[5] R.C.G.M. Loonen, M. Trčka, D. Cóstola, J.L.M. Hensen, Climate adaptive building shells: state-of-the-art and future challenges, Renew. Sustain. Energy Rev. 25 (2013) 483–493, https://doi.org/10.1016/j.rser.2013.04.016.

[6] J. Pruvost, B. Le Gouic, O. Lepine, J. Legrand, F. Le Borgne, Microalgae culture in building-integrated photobioreactors: biomass production modelling and energetic analysis, Chem. Eng. J. 284 (2016) 850–861, https://doi.org/10.1016/j.cej.2015.08.118.

[7] N. Biloria, Y. Thakkar, Integrating algae building technology in the built environment: a cost and benefit perspective, Front. Archit. Res. 9 (2020) 370–384, https://doi.org/10.1016/j.foar.2019.12.004.

[8] G.M. Elrayies, Microalgae: prospects for greener future buildings, Renew. Sustain. Energy Rev. 81 (2018) 1175–1191, https://doi.org/10.1016/j.rser.2017.08.032.

[9] R.C. Sardá, C.A. Vicente, Case studies on the architectural integration of photobioreactors in building Façades, in: F. Pacheco Torgal, C. Buratti, S. Kalaiselvam, C.G. Granqvist, V. Ivanov (Eds.), Nano Biotech Based Mater. Energy Build. Effic., Springer, Cham, 2016, pp. 1–496, https://doi.org/10.1007/978-3-319-27505-5.

[10] S. Öncel, A. Köse, D. Öncel, Façade integrated photobioreactors for building energy efficiency, in: F. Pacheco-Torgal, E. Rasmussen, C.-G. Granqvist, V. Ivanov, A. Kaklauskas, S. Makonin (Eds.), Start-Up Creat. Smart Eco-Efficient Built Environ., Woodhead Publishing, 2016, pp. 237–299, https://doi.org/10.1016/B978-0-08-100546-0.00011-X.

[11] L. Brennan, P. Owende, Biofuels from microalgae-A review of technologies for production, processing, and extractions of biofuels and co-products, Renew. Sustain. Energy Rev. 14 (2010) 557–577, https://doi.org/10.1016/j.rser.2009.10.009.

[12] V.G. Dovì, F. Friedler, D. Huisingh, J.J. Klemeš, Cleaner energy for sustainable future, J. Clean. Prod. 17 (2009) 889–895, https://doi.org/10.1016/j.jclepro.2009.02.001.

[13] K.K. Sharma, H. Schuhmann, P.M. Schenk, High lipid induction in microalgae for biodiesel production, Energies 5 (2012) 1532–1553, https://doi.org/10.3390/en5051532.

[14] M. Decker, G. Hahn, L.M. Harris, Bio-enabled façade systems managing complexity of life through emergent technologies, in: Complex. Simplicity - Proc. 34th ECAADe Conf., 1, 2016, pp. 603–612. http://papers.cumincad.org/cgi-bin/works/paper/ecaade2016_102.

[15] S.S. de Jesus, G.F. Ferreira, L.S. Moreira, R.M. Filho, Biodiesel production from microalgae by direct transesterification using green solvents, Renew. Energy 160 (2020) 1283–1294, https://doi.org/10.1016/j.renene.2020.07.056.

[16] B. Miyawaki, A.B. Mariano, J.V.C. Vargas, W. Balmant, A.C. Defrancheschi, D. O. Corrêa, B. Santos, N.F.H. Selesu, J.C. Ordonez, V.M. Kava, Microalgae derived biomass and bioenergy production enhancement through biogas purification and wastewater treatment, Renew. Energy 163 (2021) 1153–1165, https://doi.org/10.1016/j.renene.2020.09.045.

[17] A. Chemodanov, A. Robin, A. Golberg, Design of marine macroalgae photobioreactor integrated into building to support seagriculture for biorefinery and bioeconomy, Bioresour. Technol. 241 (2017) 1084–1093, https://doi.org/10.1016/j.biortech.2017.06.061.

[18] M. Zollmann, H. Traugott, A. Chemodanov, A. Liberzon, A. Golberg, Exergy efficiency of solar energy conversion to biomass of green macroalgae Ulva (Chlorophyta) in the photobioreactor, Energy Convers. Manag. 167 (2018) 125–133, https://doi.org/10.1016/j.enconman.2018.04.090.

[19] A. Elnokaly, I. Keeling, An empirical study investigating the impact of micro-algal technologies and their application within intelligent building fabrics, Procedia - Soc. Behav. Sci. 216 (2016) 712–723, https://doi.org/10.1016/j.sbspro.2015.12.067.

[20] S.L. Pagliolico, V.R.M. Lo Verso, F. Bosco, C. Mollea, C. La Forgia, A novel photo-bioreactor application for microalgae production as a shading system in buildings, Energy Procedia 111 (2017) 151–160, https://doi.org/10.1016/j.egypro.2017.03.017.

[21] F. Bumbak, S. Cook, V. Zachleder, S. Hauser, K. Kovar, Best practices in heterotrophic high-cell-density microalgal processes: achievements, potential and possible limitations, Appl. Microbiol. Biotechnol. 91 (2011) 31–46, https://doi.org/10.1007/s00253-011-3311-6.

[22] R.B. Draaisma, R.H. Wijffels, P.M. Slegers, L.B. Brentner, A. Roy, M.J. Barbosa, Food commodities from microalgae, Curr. Opin. Biotechnol. 24 (2013) 169–177, https://doi.org/10.1016/j.copbio.2012.09.012.

[23] M.R. Brown, S.W. Jeffrey, J.K. Volkman, G.A. Dunstan, Nutritional properties of microalgae for mariculture, Aquaculture 151 (1997) 315–331, https://doi.org/10.1016/S0044-8486(96)01501-3.

[24] M.A. Borowitzka, Limits to growth, in: Y.-S.W.F.Y. Tam (Ed.), Wastewater Treat. With Algae. Biotechnol. Intell. Unit, Springer, Berlin, Heidelberg, 1998, pp. 203–226, https://doi.org/10.1007/978-3-662-10863-5_12.

[25] H. Vieira de Mendonça, P. Assemany, M. Abreu, E. Couto, A.M. Maciel, R. L. Duarte, M.G. Barbosa dos Santos, A. Reis, Microalgae in a global world: new solutions for old problems? Renew. Energy 165 (2021) 842–862, https://doi.org/10.1016/j.renene.2020.11.014.

[26] D. Ying, Y. Tang, K. Shiong, K. Wayne, Y. Tao, S. Ho, Bioresource Technology Potential utilization of bioproducts from microalgae for the quality enhancement of natural products, Bioresour. Technol. 304 (2020) 122997, https://doi.org/10.1016/j.biortech.2020.122997.

[27] A. Arcos-Vargas, A. Gomez-Exposito, F. Gutierrez-Garcia, Self-sufficient renewable energy supply in urban areas: application to the city of Seville, Sustain. Cities Soc. 46 (2019) 101450, https://doi.org/10.1016/j.scs.2019.101450.

[28] M. Talaei, M. Mahdavinejad, R. Azari, Thermal and energy performance of algae bioreactive façades: a review, J. Build. Eng. (2019) 101011, https://doi.org/10.1016/j.jobe.2019.101011.
[29] E. Negev, A. Yezioro, M. Polikovsky, A. Kribus, J. Cory, L. Shashua-Bar, A. Golberg, Algae Window for reducing energy consumption of building structures in the Mediterranean city of Tel-Aviv, Israel, Energy Build. 204 (2019) 109460, https://doi.org/10.1016/j.enbuild.2019.109460.
[30] Y.H. Lin, M. Der Lin, K.T. Tsai, M.J. Deng, H. Ishii, Multi-objective optimization design of green building envelopes and air conditioning systems for energy conservation and CO2 emission reduction, Sustain. Cities Soc. 64 (2021) 102555, https://doi.org/10.1016/j.scs.2020.102555.
[31] F. Yang, F. Yuan, F. Qian, Z. Zhuang, J. Yao, Summertime thermal and energy performance of a double-skin green facade: a case study in Shanghai, Sustain. Cities Soc. 39 (2018) 43–51, https://doi.org/10.1016/j.scs.2018.01.049.
[32] M. Chàfer, L.F. Cabeza, A.L. Pisello, C.L. Tan, N.H. Wong, Trends and gaps in global research of greenery systems through a bibliometric analysis, Sustain. Cities Soc. 65 (2021), https://doi.org/10.1016/j.scs.2020.102608.
[33] F. Convertino, G. Vox, E. Schettini, Thermal barrier effect of green façades: long-wave infrared radiative energy transfer modelling, Build. Environ. 177 (2020) 106875, https://doi.org/10.1016/j.buildenv.2020.106875.
[34] H.E. Raha, M.B. Shafii, R. Roshandel, Energy efficient cultivation of microalgae using phosphorescence materials and mirrors, Sustain. Cities Soc. 41 (2018) 449–454, https://doi.org/10.1016/j.scs.2018.06.002.
[35] S.S. Oncel, A. Kose, D.S. Oncel, Carbon sequestration in microalgae photobioreactors building integrated, in: F. Pacheco-Torgal, E. Rasmussen, C.-G. Granqvist, V. Ivanov, A. Kaklauskas, S. Makonin (Eds.), Start-Up Creat. Smart Eco-Efficient Built Environ, second ed., Elsevier Ltd, 2020, pp. 161–200, https://doi.org/10.1016/B978-0-12-819946-6.00008-4.
[36] E.S. Umdu, İ. Kahraman, N. Yildirim, L. Bilir, Optimization of microalgae panel bioreactor thermal transmission property for building façade applications, Energy Build. 175 (2018) 113–120, https://doi.org/10.1016/j.enbuild.2018.07.027.
[37] M. Kerner, T. Gebken, I. Sundarrao, S. Hindersin, D. Sauss, Development of a control system to cover the demand for heat in a building with algae production in a bioenergy façade, Energy Build. 184 (2019) 65–71, https://doi.org/10.1016/j.enbuild.2018.11.030.
[38] S.L. Pagliolico, V.R.M. Lo Verso, M. Zublena, L. Giovannini, Preliminary results on a novel photo-bio-screen as a shading system in a kindergarten: visible transmittance, visual comfort and energy demand for lighting, Sol. Energy 185 (2019) 41–58, https://doi.org/10.1016/j.solener.2019.03.095.
[39] V.R.M. Lo Verso, M.H.S. Javadi, S.L. Pagliolico, C. Carbonaro, G. Sassi, Photobioreactors as a dynamic shading system conceived for an outdoor workspace of the state library of queensland in brisbane: study of daylighting performances, J. Daylighting. 6 (2019) 148–168, https://doi.org/10.15627/jd.2019.14.
[40] Y. Fang, S. Cho, Design optimization of building geometry and fenestration for daylighting and energy performance, Sol. Energy 191 (2019) 7–18, https://doi.org/10.1016/j.solener.2019.08.039.
[41] A. Zhang, R. Bokel, A. van den Dobbelsteen, Y. Sun, Q. Huang, Q. Zhang, Optimization of thermal and daylight performance of school buildings based on a multi-objective genetic algorithm in the cold climate of China, Energy Build. 139 (2017) 371–384, https://doi.org/10.1016/j.enbuild.2017.01.048.
[42] S. Carlucci, G. Cattarin, F. Causone, L. Pagliano, Multi-objective optimization of a nearly zero-energy building based on thermal and visual discomfort minimization using a non-dominated sorting genetic algorithm (NSGA-II), Energy Build. 104 (2015) 378–394, https://doi.org/10.1016/j.enbuild.2015.06.064.
[43] B. Lartigue, B. Lasternas, V. Loftness, Indoor and Built Multi-Objective Optimization of Building Envelope for Energy Consumption and Daylight, 23, 2014, pp. 70–80, https://doi.org/10.1177/1420326X13480224.
[44] R.A. Mangkuto, M. Rohmah, A.D. Asri, Design optimisation for window size, orientation, and wall reflectance with regard to various daylight metrics and lighting energy demand: a case study of buildings in the tropics, Appl. Energy 164 (2016) 211–219, https://doi.org/10.1016/j.apenergy.2015.11.046.
[45] J. Zhao, Y. Du, Multi-objective optimization design for windows and shading configuration considering energy consumption and thermal comfort: a case study for office building in different climatic regions of China, Sol. Energy 206 (2020) 997–1017, https://doi.org/10.1016/j.solener.2020.05.090.
[46] K. Konis, A. Gamas, K. Kensek, Passive performance and building form: an optimization framework for early-stage design support, Sol. Energy 125 (2016) 161–179, https://doi.org/10.1016/j.solener.2015.12.020.
[47] A. Ebrahimi-Moghadam, P. Ildarabadi, K. Aliakbari, F. Fadaee, Sensitivity analysis and multi-objective optimization of energy consumption and thermal comfort by using interior light shelves in residential buildings, Renew. Energy 159 (2020) 736–755, https://doi.org/10.1016/j.renene.2020.05.127.
[48] S. Chang, D. Castro-Lacouture, Y. Yamagata, Decision support for retrofitting building envelopes using multi-objective optimization under uncertainties, J. Build. Eng. 32 (2020) 101413, https://doi.org/10.1016/j.jobe.2020.101413.
[49] P. Pilechiha, M. Mahdavinejad, F. Pour Rahimian, P. Carnemolla, S. Seyedzadeh, Multi-objective optimisation framework for designing office windows: quality of view, daylight and energy efficiency, Appl. Energy 261 (2020) 114356, https://doi.org/10.1016/j.apenergy.2019.114356.
[50] T. Méndez Echenagucia, A. Capozzoli, Y. Cascone, M. Sassone, The early design stage of a building envelope: multi-objective search through heating, cooling and lighting energy performance analysis, Appl. Energy 154 (2015) 577–591, https://doi.org/10.1016/j.apenergy.2015.04.090.
[51] H.J. Kwon, S.H. Yeon, K.H. Lee, K.H. Lee, Evaluation of building energy saving through the development of Venetian blinds' optimal control algorithm according to the orientation and window-to-wall ratio, Int. J. Thermophys. 39 (2018), https://doi.org/10.1007/s10765-017-2350-3.
[52] C. Kasinalis, R.C.G.M. Loonen, D. Cóstola, J.L.M. Hensen, Framework for assessing the performance potential of seasonally adaptable facades using multi-objective optimization, Energy Build. 79 (2014) 106–113, https://doi.org/10.1016/j.enbuild.2014.04.045.
[53] J. Xu, J.H. Kim, H. Hong, J. Koo, A systematic approach for energy efficient building design factors optimization, Energy Build. 89 (2015) 87–96, https://doi.org/10.1016/j.enbuild.2014.12.022.
[54] M. Hamdy, A. Hasan, K. Siren, A multi-stage optimization method for cost-optimal and nearly-zero-energy building solutions in line with the EPBD-recast 2010, Energy Build. 56 (2013) 189–203, https://doi.org/10.1016/j.enbuild.2012.08.023.
[55] I.G. Dino, G. Üçoluk, Multiobjective design optimization of building space layout, energy, and daylighting performance, J. Comput. Civ. Eng. 31 (2017), https://doi.org/10.1061/(asce)cp.1943-5487.0000669, 04017025.
[56] Y. Zhai, Y. Wang, Y. Huang, X. Meng, A multi-objective optimization methodology for window design considering energy consumption, thermal environment and visual performance, Renew. Energy 134 (2019) 1190–1199, https://doi.org/10.1016/j.renene.2018.09.024.
[57] E.D. Giouri, M. Tenpierik, M. Turrin, Zero energy potential of a high-rise office building in a Mediterranean climate: using multi-objective optimization to understand the impact of design decisions towards zero-energy high-rise buildings, Energy Build. 209 (2020) 109666, https://doi.org/10.1016/j.enbuild.2019.109666.
[58] L. Magnier, F. Haghighat, Multiobjective optimization of building design using TRNSYS simulations, genetic algorithm, and Artificial Neural Network, Build. Environ. 45 (2010) 739–746, https://doi.org/10.1016/j.buildenv.2009.08.016.
[59] K. Bamdad, M.E. Cholette, L. Guan, J. Bell, Ant colony algorithm for building energy optimisation problems and comparison with benchmark algorithms, Energy Build. 154 (2017) 404–414, https://doi.org/10.1016/j.enbuild.2017.08.071.
[60] M. Marzouk, M. ElSharkawy, A. Eissa, Optimizing thermal and visual efficiency using parametric configuration of skylights in heritage buildings, J. Build. Eng. 31 (2020) 101385, https://doi.org/10.1016/j.jobe.2020.101385.
[61] B. Chegari, M. Tabaa, E. Simeu, F. Moutaouakkil, H. Medromi, Multi-objective optimization of building energy performance and indoor thermal comfort by combining artificial neural networks and metaheuristic algorithms, Energy Build. 239 (2021) 110839, https://doi.org/10.1016/j.enbuild.2021.110839.
[62] D.E. Knebel, T.P. Mcdowell, S.J. Emmerich, D.M. Brundage, J.M. Ferguson, M. W. Gallagher, W.T. Grondzik, S.S. Hanson, R.L. Hedrick, J. Humble, Standard method of test for the evaluation of building energy analysis computer programs, ASHRAE Stand 2017 (2004) 404–636.
[63] A. Szparaga, M. Stachnik, E. Czerwińska, S. Kocira, M. Dymkowska-Malesa, M. Jakubowski, Multi-objective optimization based on the utopian point method applied to a case study of osmotic dehydration of plums and its storage, J. Food Eng. 245 (2019) 104–111, https://doi.org/10.1016/j.jfoodeng.2018.10.014.
[64] N. Gunantara, A review of multi-objective optimization: methods and its applications, Cogent Eng 5 (2018) 1–16, https://doi.org/10.1080/23311916.2018.1502242.
[65] Y. Geng, B. Lin, Y. Zhu, Comparative study on indoor environmental quality of green office buildings with different levels of energy use intensity, Build. Environ. 168 (2020) 106482, https://doi.org/10.1016/j.buildenv.2019.106482.
[66] P. Shen, Z. Wang, How neighborhood form in fl uences building energy use in winter design condition: case study of Chicago using CFD coupled simulation, J. Clean. Prod. 261 (2020) 121094, https://doi.org/10.1016/j.jclepro.2020.121094.
[67] C.F. Reinhart, J. Mardaljevic, Z. Rogers, Dynamic daylight performance metrics for sustainable building design, LEUKOS J. Illum. Eng. Soc. North Am. 3 (2006) 7–31, https://doi.org/10.1582/LEUKOS.2006.03.01.001.
[68] A. Nabil, J. Mardaljevic, Useful daylight illuminance: a new paradigm for assessing daylight in buildings, Light. Res. Technol. 37 (2005), https://doi.org/10.1191/1365782805li128oa.
[69] J. de S. Freitas, J. Cronemberger, R.M. Soares, C.N.D. Amorim, Modeling and assessing BIPV envelopes using parametric Rhinoceros plugins Grasshopper and Ladybug, Renew. Energy 160 (2020) 1468–1479, https://doi.org/10.1016/j.renene.2020.05.137.
[70] M.S. Roudsari, M. Pak, Ladybug, A parametric environmental plugin FORfor grasshopperto help designers creat an environmentally-conscious design, in: BS2013-13th Int. Conf. Build. Perform. Simul. Assoc., Chambery, France, 2013, pp. 3128–3135.
[71] Y. Zhai, Y. Wang, Y. Huang, X. Meng, A multi-objective optimization methodology for window design considering energy consumption, thermal environment and visual performance, Renew. Energy 134 (2019) 1190–1199, https://doi.org/10.1016/j.renene.2018.09.024.
[72] C.F. Reinhart, O. Walkenhorst, Validation of dynamic RADIANCE-based daylight simulations for a test office with external blinds, Energy Build. 33 (2001) 683–697, https://doi.org/10.1016/S0378-7788(01)00058-5.
[73] Climate.onebuilding.org, 2020. http://climate.onebuilding.org/WMO_Region_2_Asia/IRN_Iran/index.html. (Accessed 8 June 2020).
[74] Energy Standard for Buildings except Low-Rise Residential Buildings, ASHRAE Stand, 2013.
[75] M. Talaei, M. Mahdavinejad, A. Zarkesh, H. Motevali Haghighi, A review on interaction of innovative building envelope technologies and solar energy Gain, in: Energy Procedia, 2017, https://doi.org/10.1016/j.egypro.2017.11.006.

[76] S.W.K. Jung Hwa Lee, Jin Suk Lee, Chul Seung Shin, Soon Chul Park, Effects of NO and SO2 on growth of highly-CO2-tolerant microalgae, J. Microbiol. Biotechnol. 10 (2000) 338–343.
[77] E. Ortiz, A. Converti, A.A. Casazza, E.Y. Ortiz, P. Perego, M. Del Borghi, Effect of temperature and nitrogen concentration on the growth and lipid content of Nannochloropsis oculata and Chlorella vulgaris for biodiesel production, Chem. Eng. Process. Process Intensif. 48 (2009) 1146–1151, https://doi.org/10.1016/j.cep.2009.03.006.
[78] A.W. Mayo, Effects of temperature and pH on the kinetic growth of unialga Chiarella vulgaris cultures containing bacteria, Water Environ. Res. 69 (1997) 64–72. http://hdl.handle.net/20.500.11810/2234.
[79] R. Evins, A review of computational optimisation methods applied to sustainable building design, Renew. Sustain. Energy Rev. 22 (2013) 230–245, https://doi.org/10.1016/j.rser.2013.02.004.
[80] S. Bandyopadhyay, S. Saha, Some single- and multiobjective optimization, in: Unsupervised Classif, Springer, Berlin, Heidelberg, 2013, pp. 17–58, https://doi.org/10.1007/978-3-642-32451-2_2.
[81] S. Seyedzadeh, F. Pour Rahimian, Multi-objective optimisation and building retrofit planning, in: Green Energy Technol., Springer Science and Business Media Deutschland GmbH, 2021, pp. 31–39, https://doi.org/10.1007/978-3-030-64751-3_3.
[82] A.F. Ali, M.A. Tawhid, A hybrid particle swarm optimization and genetic algorithm with population partitioning for large scale optimization problems, Ain Shams Eng. J. 18 (2017) 191–206, https://doi.org/10.1016/j.asej.2016.07.008.
[83] N.C. Brown, V. Jusiega, C.T. Mueller, Implementing data-driven parametric building design with a flexible toolbox, Autom. ConStruct. 118 (2020) 103252, https://doi.org/10.1016/j.autcon.2020.103252.
[84] N. Brown, J. Ochsendorf, C. Mueller, J. de Oliveira, Early-stage integration of architectural and structural performance in a parametric multi-objective design tool, in: Struct. Archit. - Proc. 3rd Int. Conf. Struct. Archit. ICSA 2016, CRC Press/Balkema, 2016, pp. 1103–1111, https://doi.org/10.1201/b20891-152.
[85] M. Kim, T. Hiroyasu, M. Miki, S. Watanabe, SPEA2+: improving the performance of the strength pareto evolutionary algorithm 2, Lect. Notes Comput. Sci. 3242 (2004) 742–751, https://doi.org/10.1007/978-3-540-30217-9_75.
[86] C. Sun, Q. Liu, Y. Han, Many-objective optimization design of a public building for energy, daylighting and cost performance improvement, Appl. Sci. 10 (2020), https://doi.org/10.3390/app10072435.
[87] K. Bringmann, T. Friedrich, C. Igel, T. Voß, Speeding up many-objective optimization by Monte Carlo approximations, Artif. Intell. 204 (2013) 22–29, https://doi.org/10.1016/j.artint.2013.08.001.
[88] D. Luengo, L. Martino, M. Bugallo, V. Elvira, S. Särkkä, A survey of Monte Carlo methods for parameter estimation, EURASIP J. Appl. Signal Process. 2020 (2020) 1–62, https://doi.org/10.1186/s13634-020-00675-6.
[89] D.P. Morton, E. Popova, Monte—carlo simulations for stochastic optimization, in: Encycl. Optim., Springer US, 2006, pp. 1529–1537, https://doi.org/10.1007/0-306-48332-7_305.
[90] R.M. Everson, J.E. Fieldsend, S. Singh, Full elite sets for multi-objective optimisation, in: Adapt. Comput. Des. Manuf. V, Springer London, 2002, pp. 343–354, https://doi.org/10.1007/978-0-85729-345-9_29.
[91] L. While, P. Hingston, L. Barone, S. Huband, A faster algorithm for calculating hypervolume, IEEE Trans. Evol. Comput. 10 (2006) 29–38, https://doi.org/10.1109/TEVC.2005.851275.
[92] L.D. Hernández, S. Moral, A. Salmerón, A Monte Carlo algorithm for probabilistic propagation in belief networks based on importance sampling and stratified simulation techniques, Int. J. Approx. Reason. 18 (1998) 53–91, https://doi.org/10.1016/S0888-613X(97)10004-4.
[93] M. Cervantes, The Monte Carlo method, Math. Sci. Eng. 92 (1972) 181–208, https://doi.org/10.1016/S0076-5392(08)61352-1.
[94] P. Bakmohammadi, E. Noorzai, Optimization of the design of the primary school classrooms in terms of energy and daylight performance considering occupants' thermal and visual comfort, Energy Rep. 6 (2020) 1590–1607, https://doi.org/10.1016/j.egyr.2020.06.008.
[95] Y. Shahbazi, M. Heydari, F. Haghparast, An early-stage design optimization for office buildings' façade providing high-energy performance and daylight, Indoor Built Environ. 28 (2019) 1350–1367, https://doi.org/10.1177/1420326X19840761.
[96] E. Touloupaki, T. Theodosiou, Optimization of building form to minimize energy consumption through parametric modelling, Procedia Environ. Sci. 38 (2017) 509–514, https://doi.org/10.1016/j.proenv.2017.03.114.
[97] R. Vierlinger, Multi Objective Design Interface, University of Applied Arts Vienna, 2013, https://doi.org/10.13140/RG.2.1.3401.0324.
[98] L.J. Eshelman, J.D. Schaffer, Real-Coded Genetic Algorithms and Interval-Schemata, Elsevier, 1993, pp. 187–202, https://doi.org/10.1016/b978-0-08-094832-4.50018-0.
[99] Z. Kaseb, M. Hafezi, M. Tahbaz, S. Delfani, A framework for pedestrian-level wind conditions improvement in urban areas: CFD simulation and optimization, Build. Environ. 184 (2020) 107191, https://doi.org/10.1016/j.buildenv.2020.107191.
[100] C.K. LaDue, V.V. Sapozhnykov, K.S. Fienberg, A data modem for GSM voice channel, IEEE Trans. Veh. Technol. 57 (2008) 2205–2218, https://doi.org/10.1109/TVT.2007.912322.
[101] A. Ruiz-Marin, L.G. Mendoza-Espinosa, T. Stephenson, Growth and nutrient removal in free and immobilized green algae in batch and semi-continuous cultures treating real wastewater, Bioresour. Technol. 101 (2010) 58–64, https://doi.org/10.1016/j.biortech.2009.02.076.
[102] L. Zhu, Z. Wang, J. Takala, E. Hiltunen, L. Qin, Z. Xu, X. Qin, Z. Yuan, Bioresource Technology Scale-up potential of cultivating Chlorella zofingiensis in piggery wastewater for biodiesel production, Bioresour. Technol. 137 (2013) 318–325, https://doi.org/10.1016/j.biortech.2013.03.144.
[103] L. Zhu, Microalgal culture strategies for biofuel production: a review, Microalgal Cult. Strateg. 9 (2015) 801–814, https://doi.org/10.1002/bbb.1576.
[104] A. Köse, S.S. Öncel, Photobioreactors for sustainable buildings, Deu Muhendis. Fak. Fen ve Muhendis. 18 (2016), https://doi.org/10.21205/deufmd.20165217548, 77–77.
[105] M. Casini, Smart Buildings Advanced Materials and Nanotechnology to Improve Energy-Efficiency and Environmental Performance, first ed., Woodhead Publishing, 2016.
[106] Z. Pang, Z. O'Neill, Y. Li, F. Niu, The role of sensitivity analysis in the building performance analysis: a critical review, Energy Build. 209 (2020) 109659, https://doi.org/10.1016/j.enbuild.2019.109659.
[107] N. Delgarm, B. Sajadi, K. Azarbad, S. Delgarm, Sensitivity analysis of building energy performance: a simulation-based approach using OFAT and variance-based sensitivity analysis methods, J. Build. Eng. 15 (2018) 181–193, https://doi.org/10.1016/j.jobe.2017.11.020.
[108] H. Li, S. Wang, H. Cheung, Sensitivity analysis of design parameters and optimal design for zero/low energy buildings in subtropical regions, Appl. Energy 228 (2018) 1280–1291, https://doi.org/10.1016/j.apenergy.2018.07.023.
[109] X. Song, J. Zhang, C. Zhan, Y. Xuan, M. Ye, C. Xu, Global sensitivity analysis in hydrological modeling: review of concepts, methods, theoretical framework, and applications, J. Hydrol 523 (2015) 739–757, https://doi.org/10.1016/j.jhydrol.2015.02.013.
[110] A. Saltelli, M. Ratto, T. Andres, F. Campolongo, J. Cariboni, D. Gatelli, Michaela Saisana, S. Tarantola, Global Sensitivity Analysis. The Primer, John Wiley & Sons, 2008, https://doi.org/10.1002/9780470725184.
[111] M.K. Kim, Y.S. Kim, J. Srebric, Predictions of electricity consumption in a campus building using occupant rates and weather elements with sensitivity analysis: artificial neural network vs. linear regression, Sustain. Cities Soc. 62 (2020) 102385, https://doi.org/10.1016/j.scs.2020.102385.
[112] G. Ciulla, A. D'Amico, Building energy performance forecasting: a multiple linear regression approach, Appl. Energy 253 (2019) 113500, https://doi.org/10.1016/j.apenergy.2019.113500.
[113] T. Wei, A review of sensitivity analysis methods in building energy analysis, Renew. Sustain. Energy Rev. 20 (2013) 411–419, https://doi.org/10.1016/j.rser.2012.12.014.
[114] R. Singh, I.J. Lazarus, V.V.N. Kishore, Uncertainty and sensitivity analyses of energy and visual performances of office building with external Venetian blind shading in hot-dry climate, Appl. Energy 184 (2016) 155–170, https://doi.org/10.1016/j.apenergy.2016.10.007.
[115] P. Hoseinzadeh, M. Khalaji, S. Heidari, M. Khalatbari, R. Saidur, K. Haghighat, H. Sangin, Energy performance of building integrated photovoltaic high-rise building: case study, Tehran , Iran, Energy Build. 235 (2021) 110707, https://doi.org/10.1016/j.enbuild.2020.110707.